Appendix Supporting Information

SI Materials and Methods.

Animal procedures

The generation and characterization of Tg mice with Thy1.2 promoter driven expression of untagged WT UBQLN2 (Line 356) or ALS/FTD mutant P497S UBQLN2 protein (Line P497S) were described previously (1). The two lines were backcrossed with C57BL/6 mice for at least 10 generations prior to use for the present study. The Non-Tg mice were the C57BL/6J strain (Stock 000664) from The Jackson Laboratory (The Jackson Laboratory, Bar Harbor, ME). The procedure for genotyping the UBQLN2 transgenic mice was described previously (1).

Mice with germ-line inactivation of UBQLN2 were generated by cre-induced deletion of the UBQLN2 open-reading frame that had been “floxed” in ES cells. The UBQLN2-deleted ES cells were used to derive UBQLN2 KO mice (2).

All animal procedures were approved by University of Maryland Baltimore (UBQLN2 Tg mice) and Harvard University (UBQLN2 KO mice) Animal Care and Use Committees and conducted in full accordance with the NIH Guide for the Care and Use of Laboratory Animals.

Expression and purification of recombinant proteins

Human cDNA encoding the complete open reading frame of ATP6v1g1 was cloned between the KpnI and XhoI sites in pET-45b (Millipore-Sigma) to express a His-tagged fusion protein. The expression plasmid was transformed into Rosetta (DE3) cells

and the His-ATP6v1g1 fusion protein induced by addition of 1 mM IPTG for 4 hours at 30ºC. The His-ATP6v1g1 fusion protein was purified from the induced bacteria using Ni-NTA agarose (Qiagen, Germantown, MD, USA) according to the manufacturer's instructions. Full-length (FL) WT UBQLN2-GST fusion protein and corresponding proteins carrying one of 5 different ALS/FTD mutations (P497H, P497S, P506T, P509S, and P525S) were expressed in BL21 (DE3) bacteria and the GST-fusion proteins were purified using Glutathione-Agarose (Sigma-Millipore) as described before (3). Both GST and His purified proteins were dialyzed against dialysis buffer (10% glycerol, 20 mm Tris pH 8.0 and 150 mm NaCl) and stored at -80ºC until use.

GST-pulldown assays

MagneGST beads (Promega, Madison, WI, USA) (400 μl) were washed twice and then resuspended in their original volume with GST pulldown buffer (50 mM Tris-HCl pH 7.5, 150 mM NaCl, 2 mM EDTA, 1 mM DTT, 1% NP40). Aliquots (40 μl) of this suspension were then mixed with 500 μl of the GST-pulldown buffer containing 0.4% BSA and 10 μg amounts of different GST-UBQLN2 fusion proteins or with GST alone for 2 hours at 4ºC, with rotation. Meanwhile 25 μg of His-ATP6v1g1 purified protein was incubated under the same conditions with 40 μl of the resuspended MagneGST beads and 1 ml of GST pulldown buffer containing 0.4% BSA. The beads were then captured onto the side of the tubes with a magnet and the supernatant was replaced with 400 μl of fresh GST pulldown buffer containing 0.4% BSA. Likewise, the beads were separated from the tube containing His-ATP6v1g1 and 140 μl aliquots of the supernatant were added to each tube containing the different GST-bound proteins. The mixtures were

then rotated for 2 hours at 4ºC after which the beads were washed 5 times with plain GST-pulldown buffer and finally resuspended in 150 μl of 50 mM Tris-HCL pH 6.8 and 50 μl of SDS loading buffer. The mixtures were gently vortexed and the beads pelleted by centrifugation at 5,000 g for 5 min. Equal portion of the mixtures were then separated by SDS-PAGE and analyzed for ATP6v1g1-HIS binding by immunoblotting for both the GST fusion proteins and the ATP6v1g1 subunit.

Construction of Venus reporter plasmids for monitoring autophagosome targeting and maturation

The pDest-mCherry-EGFP-LC3B construct (4) was kindly provided by Dr. Terje Johansen, University of Tromso, Norway. N and CVenus expression constructs were obtained from addgene (plasmids #27097 and 22011). Standard PCR and molecular biology procedures were used to generate the remaining expression constructs. NVenus-tagged UBQLN2 expression constructs were constructed by cloning the cDNA fragment encoding amino acids 1-155 of NVenus, containing the I152L mutation that reduces self-assembly and decreases background fluorescence (5, 6), upstream and in-frame with UBQLN2 cDNAs encoding either full-length WT human UBQLN2 or carrying one of five different ALS/FTD UBQLN2 mutations (P497H, P497S, P506T, P509S and P525S mutations). A spacer containing 2 glycine residues was introduced between the N-Venus and UBQLN2 fusions. The complementary CVenus 82 amino acid fragment was fused with LC3B either with or without mCherry. In one version, LC3B as fused downstream of CVenus with a 5-glycine spacer between the two proteins to generate CVenus-LC3B. A second version was made by inserting mCherry between CVenus-

LC3B generating CVenus-mCherry-LC3B. The constructs were verified by DNA sequencing and by production of the correct size polypeptides following transfection and immunoblotting.

Construction of HA and Myc-tagged UBQLN2 and ATP6v1g1 mammalian expression constructs

The cDNA encoding the complete human ATP6v1g1 open reading frame was cloned between the ApaI and XhoI sites in the pCMV-Myc-C vector (Clontech Laboratories Inc., Mountain View, CA) to express ATP6v1g1 with a C-terminal Myc-tag. WT and ALS/FTD mutant UBQLN2 proteins were expressed as N-terminal HA-tagged proteins as described previously (3). For the studies investigating the effects of UBQLN2 expression on ATP6v1g1 biogenesis, the total amount of plasmid DNA transfected in each dish was kept constant by adjusting the amount of empty vector plasmid that was transfected. A plasmid encoding EGFP-C1 (Clontech) was used as a control to determine the specificity of any UBQLN2-dependent regulation of its expression and to monitor the efficiency of cell transfection.

Immunoprecipitation studies

HeLa cells grown in 100 mm dishes were transfected with plasmids encoding the different proteins shown and the next day the cells were washed two times with ice-cold 1 x PBS and then scraped from the dishes after addition of 1 ml of RIPA buffer (50 mM Tris-HCl pH 7.5, 150 mM NaCl, 2 mM EDTA, 1mM Pefabloc, 1% NP40) and sheared 20 times through a 25-gage needle. A 100 μl aliquot was saved to assess expression of the

constructs and the remainder was divided into 2 equal portions to conduct immunoprecipitations using either mouse anti-UBQLN2 or control IgG antibodies using the method described previously (3). Additional immunoprecipitations were conducted using rabbit anti-HA and rabbit anti-Myc antibodies (both produced in house). Equal portions (1/10) of the immunoprecipitations and 5 to 10 μl sample of the lysates were analyzed for immunoprecipitation and coimmunoprecipitation of the different proteins shown.

Preparation of protein lysates, SDS-PAGE and immunoblotting procedures

Protein lysates from cell cultures were prepared by washing the cultures twice with ice-cold 1 x PBS followed by lysis with protein lysis buffer (50 mM Tris pH 6.8, 150 mM NaCl, 20 mM EDTA, 1 mM EGTA, 0.5% SDS, 0.5% NP40, sarkosyl 0.5%, 10 mM orthovanadate, 2.5 mM sodium fluoride) (7). The only exception was when we used 8 M Urea lysis buffer (8) to analyze p62 levels in the different HeLa lines. The lysates were sonicated and the protein concentration determined by the BCA method (Pierce BCA Assay kit, Thermo Fisher Scientific). Mouse tissue lysates were prepared from the brain, hippocampus, and SC of mice that had just been euthanized. The isolated tissues were homogenized at 50 rpm for 5 min with protein lysis buffer using a Kontes-type glass homogenizer with a Teflon pestle connected to a Yamato LSC homogenizer LH21. Protein concentrations of the homogenates were determined by the BCA method.

The hippocampus and lumbar portion of the spinal cord were isolated from three independent Non-Tg, WT 356 and P497S animals at 2 months of age. The proteome in these isolates were determined by isobaric labelling following by mass spectrometry

quantification. Only the results of the changes in the ATP6 subunits of the V-ATPase pump are shown. The proteome analysis of the samples that are unrelated to this publication will be deposited in the Proteome Xchange Consortium via PRIDE (PMID 26527722).

Lysates containing known amounts of protein were mixed with SDS loading buffer and the proteins were separated on 8.5 to 12.5% polyacrylamide gels by SDS-PAGE. The proteins were then transferred onto 0.45 µm PVDF membranes (Millipore, Billerica, MA, USA) for 20 to 20 min at 1.3 Amps using the Power Blotter XL System (ThermoFisher Scientific, Waltham, MA, USA) and probed for reaction with antibodies using the chemiluminescence method (7). Primary antibodies used for immunoblotting were mouse monoclonal p62 (#ab56416), rabbit anti-LC3B (#ab192890), and rabbit polyclonal anti-ATP6v1b2 (#ab73404) all from abcam (Cambridge, MA, USA), mouse monoclonal anti-UBQLN2 (#NBP2-25164, Novus Biologicals Centennial, CO, USA), mouse monoclonal anti-UBQLNs (#37-7700) and rabbit anti-Cathepsin D (PA5-72182), both from Invitrogen (Carlsbad, CA, USA), rabbit polyclonal ATP6v1g1 (#16143-1-AP) and ATP6v0a1(#13828-1-AP) both from Proteintech, Rosemont, IL, USA) mouse monoclonal ATP6v1g1 (sc-25333), goat anti-LAMP1 (sc-8098) and goat anti-actin (sc-1616) all from Santa Cruz Biotechnology (Dallas, TX, USA), rabbit anti-LC3A/B (#4108) and rabbit anti-p62 (#5114) both from Cell Signaling Technology (Danvers, MA, USA), rabbit monoclonal anti-K48 and K63 ubiquitin chains (#05-1307 and #05-1308) and mouse monoclonal Anti-WIPI2 (MABC91) all from Millipore-Sigma, Burlington, MA, USA), rabbit anti-p97/VCP (home-made) and mouse anti-GAPDH (#60004-1-Ig, Proteintech). The immunoblotting procedure involved incubating the membranes with

primary antibodies for 17 to 20 hours, which were then washed 5 times and then incubated with appropriate horseradish peroxidase-conjugated secondary antibodies (all from Thermo Fisher Scientific, Waltham, MA) for 2 h. The membranes were washed again and then incubated with a 1:1 mixture of the SuperSignal West Pico system (Thermo Fisher Scientific) and the emitted chemiluminescent signal was captured using a Fluoro-Chem M imager (Protein Simple, Santa Clara, CA, USA). The intensity of different bands of captured images were quantified using AlphaView software (Protein Simple).

Cell culture and derivation of CRISPR/Cas9 UBQLN2 KO lines

HeLa (ATCC CCL-2) and NSC34 (Cedarlane CLU140) cells were grown in DMEM supplemented with 10% fetal bovine serum at 37ºC with 5% CO_2. To generate the stable UBQLN2 knockout (KO) cell lines, HeLa and NSC34 cells were transfected with 2 µg UBQLN2 CRISPR/Cas9 KO plasmid sc-404783(human) or UBQLN2 CRISPR/Cas9 KO plasmid (mouse) sc-424895, respectively, using the calcium phosphate co-precipitation method. Twenty-four hours after transfection, cells were trypsinized, diluted 10-fold with DMEM and replated. The next day, selection media (DMEM + 2.5 µg/ml puromycin) was added to the cells. Cells were maintained in selection media, which was replaced every three to four days. Fourteen days later, individual colonies were trypsinized and replated into separate wells of a 6-well plate containing fresh selection media and allowed to grow until colonies could be expanded to 60 mm dishes. After 24 hours, lysates were collected and knock-out of UBQLN2 was

determined by immunoblotting. Two different HeLa and NSC34 UBQLN2 KO lines were used for the present study.

Generation of HeLa cells stably expressing the mCherry-EGFP-LC3 reporter and siRNA knockdown studies

A pool of HeLa cells stably expressing the autophagosome-autolysosome reporter construct (4) was made by transfecting HeLa cells with a 10 to 2 μg ratio of pDest-mCherry-EGFP-LC3b plasmid and PSV2neo by calcium phosphate transfection and then selecting cells that grew resistant to 700 μg/ml G418 (345810, Calbiochem).

Knockdown of ATP6v1g1 was conducted by transfecting the pool of HeLa cells stably expressing the pDest-mCherry-EGFP-LC3b reporter plasmid with either 10 nM siRNA specifically targeting ATP6v1g1 (L-013608-01-0005, Dharmacon Inc., Lafayette, CO) or 10 nM non-targeting siRNA (D-001810-01-05, Dharmacon Inc.) using Dharmafect 1 Reagent (T-2001-01, Dharmacon Inc.) according to the manufacture's protocol.

Analysis of Protein Turnover

HeLa or the KO8 cell line were plated at equal densities in DMEM with glucose containing 10% fetal bovine serum (FBS) and grown overnight at 37ºC with 5% CO_2. The next morning the media was replaced with fresh 37ºC-warm medium containing cycloheximide (CHX) at a concentration of 100 μg/ml and reincubated for different time periods. Cultures were removed at 2-hour intervals and protein lysates were prepared as described above.

Autophagy Flux Assays

For autophagic flux assay, cells were first plated at equal densities in DMEM with glucose containing 10% fetal bovine serum (FBS) and grown at 37ºC with 5% CO_2. The next day the cultures were quickly washed 3 times with one of three different 37ºC prewarmed solutions: either DMEM plus 10% FBS with glucose (Corning #10-017, Corning, NY), or DMEM plus 10% FBS without glucose (#11966-025, Gibco, Thermo Fisher Scientific), or in EBSS (Gibco #14155-063). After washing, the cultures were incubated with a fresh amount of the wash solution and incubated for 0, 2, and 4 hours at 37ºC without or after addition of bafilomycin A1 (Enzo Life Sciences, Farmingdale, NY) to a final concentration of 200 nM. Cultures were removed at appropriate time intervals and washed twice in ice-cold 1 x standard PBS and protein lysates were prepared as described above. Equal amounts of proteins were immunoblotted for the proteins as shown in the figures. The results shown were repeated three times, producing similar results.

DNA transfections, immunofluorescence and Venus complementation assays

All microscopic evaluation of cell staining, intracellular fluorescence and Venus complementation assays were performed by transfection of normal or UBQLN2 KO8 HeLa cells grown on coverslips. The cells were plated on glass coverslips and cultured in DMEM with glucose containing 10% fetal bovine serum (FBS) and grown overnight at 37ºC with 5% CO_2. The next day the medium was replaced with fresh medium and the cultures were transfected with the various plasmid DNAs using the calcium phosphate coprecipitation method. The next day the coverslips were dipped in 37ºC warm 1 X PBS

for 1 min and then immersed in 4% paraformaldehyde in 1 x PBS for 15 min after which they were washed 3 times in 1 x PBS and then stained. Antibody staining was performed by applying appropriate dilutions of primary antibodies in 0.8% BSA in 1 x PBS for 2 hours, then washing 5 times in 1 x PBS, followed by incubation with appropriate secondary AlexaFluor antibodies for 2 hours. The Alexa Fluor secondary antibodies used were goat anti-mouse 405 (A31553), donkey anti-goat 488 (A11055), donkey anti-mouse 488 (A21202), donkey anti-mouse 594 (A21203), donkey ant-rabbit 594 (A21207), donkey anti-rabbit 647 (A31573) and rabbit anti-goat 647 (A21446) all from Invitrogen. The coverslips were washed again 3 times in 1 x PBS, then stained for 5 min with DAPI (0.5 µg/mL) and washed again and mounted on slides using aqueous mounting medium (Aquamount, Thermo Fisher). The fluorescent images were captured using an inverted Zeiss Axiovert 200 microscope with an Acroplan 100x/1.25 oil objective using appropriate filter sets (YFP-2427B, TRIC-B, Cy5-4040C, FITC-3540C (all from Semrock) and DAPI filter set 49 (488049 Zeiss) using SimplePCI software (Hamamatsu, Sewickley, PA). The captured images were merged using iVision software. Quantification of autophagosome acidification was based on analysis of at least 5 to 10 cells.

For detection of LAMP1 staining of the cells transfected with the Venus reporters constructs, the fluorescence of the cells was first quenched by incubating the coverslips in ice cold 70% ethanol for 1 hour followed by three washes with 1 x PBS and then reincubation in 100% methanol at -20ºC for 1 hour. The coverslips were washed again and treated with a 1 x PBS solution containing 3% H_2O_2 and 20 mM NaOH for 1 hour.

The coverslips were then washed 3 times with 1 x PBS and stained using our standard protocol.

For the Lysotracker staining, cells were plated on coverslips and the next day incubated in 1 µg/ml Hoescht 33342 (B2261, Sigma Aldrich) for 5 min. The media was then changed with fresh DMEM medium containing 50 nM Lysotracker Red DND-99 (L-7528, Molecular Probes) for 10 minutes. The coverslips were washed 3 times with warm 1 x PBS and imaged using the TRIC-B filter set with a 20X/0.5 Plan-Neofluar objective. All images were captured with the same exposure settings and for identical times. The intensity of fluorescence of at least 10 cells were counted from 10 independent images for each cell line using iVision software.

Similar exposure and time settings were used to capture the fluorescence intensity for the p62 staining in the HeLa and KO8 cells. The intensity of p62 fluorescence of at least 10 cells were counted from 2 independent images. The number of p62 inclusions that were between 0.3 to 2 µm were counted for at least 8 different cells.

Mouse tissue isolation, staining and immunofluorescence microscopy

Mouse brain and spinal cords (SC) were dissected from perfused and non-perfused animals at different ages and quickly frozen on dry ice and then moved to storage at -80ºC. When needed, the brains and SCs were thawed on ice and then fixed in 4% paraformaldehyde in 1 x PBS for 24 hours at 4ºC and then transferred to a solution containing 25% sucrose in 1 x PBS for 24 hours at 4ºC. The tissues were then embedded in O.T.C. compound (Sakura Finetek USA, Inc., Torrance CA) and ~15 to 20

μm thick sections we cut with a Leica CM3050S cryostat and mounted onto slides. The procedure for immunofluorescence staining was as described previously (1, 9). Primary antibodies used for staining were: UBQLN2, p62, LC3, and ATP6v1g1. Alexafluor secondary antibodies of different wavelength (405, 488, 555 and 647 nm) were used for double immunofluorescence detection of different proteins. Following the antibody incubations, the slides were extensively washed and then briefly stained with DAPI and then coverslipped. Confocal images of the stained slides (and some of the cells transfected with the Venus reporter) were captured using a Nikon Eclipse Ti2 confocal microscope with either an Apo 60X/1.40 oil, or S Fluor 40X/1.30 oil objective equipped with 405, 488, 560 and 646 nm laser lines with tunable exciter and emitter capabilities. The confocal images were processed using iVision software (BioVision Technologies, Exton, PA).

Human Tissue samples and staining

Formalin-fixed paraffin-embedded (FFPE) hippocampal tissue from *UBQLN2*-linked ALS cases were obtained from; the UK MRC Neurodegenerative Diseases Brain Bank (Case A033_08, c.1516C>T, p.P506S (10), individual II.2); from the Feinberg School of Medicine, Northwestern University, USA (Case X11-03, c.1490C>A, p.P497H (11), Family #186, individual V:I); and from the Neurological Foundation Human Brain Bank as per sporadic cases (Case MN17, c.1460C>T, p.T487I (12, 13), individual IV:18) (n=3, mean age at death or invasive ventilation= 55.3 y, mean post-mortem delay= 21.2 h). At each site, donor and family consent and ethical approvals were obtained and clinical and neuropathological diagnoses were conducted as described previously.

Hippocampal tissue sections were cut with a microtome in the transverse plane at a thickness of 7-10 μm and mounted onto microscope slides. Mounted sections were desiccated at room temperature for a minimum of 1 week before immunohistochemistry. Slides were heated to 60 °C for 1 hour on a hot plate, then dewaxed through an alcohol-zylene-water series: 100% xylene, 2 x 30 min; 100% ethanol, 2 x 15 min; 95%, 85%, 75% ethanol, 2 min each; water 3 x 5 min. For antigen retrieval, slides were immersed in sodium citrate buffer pH 6.0 (Abcam) for 2 hours in a pressure cooker, followed by 1 x phosphate-buffered saline (PBS) washes, 3 x 5 min. Wax borders were drawn, and sections permeabilized with PBS-T (0.1% Triton X-100) for 15 min at 4 °C followed by PBS washes 3 x 5 min. Autofluorescence was quenched with 1 x TrueBlack (Biotium) in 70% EtOH for 30 sec at room temperature. Sections were blocked in 10% normal donkey serum (NDS) for 1 hour. Primary antibodies (UBQLN2, Santa Cruz SC-100612, 1:200; and p62, ProGen GP62-C, 1:300) were applied overnight in 1% NDS. Following washing, secondary Alexa Fluor 488 and 647 antibodies (Invitrogen A11001 and A21450, 1:500) were applied for 3 hours in 1% NDS. Sections were counterstained with Hoechst 33342 nuclear stain for 5 min at 0.5 μg/mL and then coverslipped. Entire hippocampal sections were imaged with a MetaSystems VSlide slide scanner at 20x magnification (0.9 NA) using MetaCyte acquisition and stitching software. DAPI (excitation band 375/38 nm), AlexaFluor 488 (484/25 nm), and Cy5 (631/22 nm) were acquired using a Colibri 2 LED light source (Zeiss). All sections were imaged with the same settings for each staining combination. Image post-processing was tailored to each section to best represent the signals for the protein inclusions.

RNA extraction and Real-Time quantitative PCR analysis

Total RNA was extracted from cells using the Absolutely RNA Nanoprep Kit (Agilent Technologies) according to the manufacturer's instructions. RNA was converted to cDNA using the reverse transcription kit obtained from Invitrogen (#4374966). RT-quantitative PCR reactions were performed using three of four biological replicates using specified primers and probes with RotorGene 3000 software (QIAgen). Relative expression fold changes were normalized to β-Actin. The following sets of primers and probes were used. Human β-Actin: IDT PrimeTime qPCR Assay Hs.PT.39a.22214847, Forward: CAACCTCTTGGCTTTTGTCTG, Reverse: AGCTTCATATTCGTGAGGGC, Probe: /56-FAM/ TCATCCATG /ZEN/ GTGAGCTGGCGG /3IABKFQ/. Human p62: IDT PrimeTime qPCR Assay Hs.PT.58.39829257, Forward: CTGCCTTGTACCCACATCTC Reverse: CCGATGTCATAGTTCTTGGTCTG, Probe: /56-FAM/ TGCTGTCCA /ZEN/ TGGGCTTCTCTGATG /3IABKFQ/.

Statistical methods

Differences in protein expression between different samples were analyzed using Student t tests using Microsoft Excel or Graphpad Prism 7 software. One-way ANOVA analysis was used to determine differences in autophagosome acidification of WT and mutant UBQLN2 proteins. $P \leq 0.05$ was considered to be statistically significant. Stat symbols used: ns = $P > 0.05$, * = $P < 0.05$, ** = $P < 0.01$, *** = $P < 0.001$, **** = $P < 0.0001$.

REFERENCES

1. N. T. Le *et al.*, Motor neuron disease, TDP-43 pathology, and memory deficits in mice expressing ALS-FTD-linked UBQLN2 mutations. *Proc Natl Acad Sci U S A* **113**, E7580-E7589 (2016).
2. A. M. Whiteley *et al.*, Ubiquilin1 promotes antigen-receptor mediated proliferation by eliminating mislocalized mitochondrial proteins. *Elife* **6** (2017).
3. L. Chang, M. J. Monteiro, Defective Proteasome Delivery of Polyubiquitinated Proteins by Ubiquilin-2 Proteins Containing ALS Mutations. *PLoS One* **10**, e0130162 (2015).
4. S. Pankiv *et al.*, p62/SQSTM1 binds directly to Atg8/LC3 to facilitate degradation of ubiquitinated protein aggregates by autophagy. *J Biol Chem* **282**, 24131-24145 (2007).
5. Y. Kodama, C. D. Hu, An improved bimolecular fluorescence complementation assay with a high signal-to-noise ratio. *Biotechniques* **49**, 793-805 (2010).
6. Y. Kodama, C. D. Hu, Bimolecular fluorescence complementation (BiFC): a 5-year update and future perspectives. *Biotechniques* **53**, 285-298 (2012).
7. J. Ugolino *et al.*, Overexpression of human Atp13a2Isoform-1 protein protects cells against manganese and starvation-induced toxicity. *PLoS One* **14**, e0220849 (2019).
8. D. M. Sampathu *et al.*, Pathological heterogeneity of frontotemporal lobar degeneration with ubiquitin-positive inclusions delineated by ubiquitin immunohistochemistry and novel monoclonal antibodies. *Am J Pathol* **169**, 1343-1352 (2006).

9. R. Starr, J. Xiao, M. J. Monteiro, Production of monoclonal antibodies against neurofilament-associated proteins: demonstration of association with neurofilaments by a coimmunoprecipitation method. *J Neurochem* **64**, 1860-1867 (1995).

10. S. A. Gkazi *et al.*, Striking phenotypic variation in a family with the P506S UBQLN2 mutation including amyotrophic lateral sclerosis, spastic paraplegia, and frontotemporal dementia. *Neurobiol Aging* **73**, 229 e225-229 e229 (2019).

11. H. X. Deng *et al.*, Mutations in UBQLN2 cause dominant X-linked juvenile and adult-onset ALS and ALS/dementia. *Nature* **477**, 211-215 (2011).

12. E. L. Scotter *et al.*, C9ORF72 and UBQLN2 mutations are causes of amyotrophic lateral sclerosis in New Zealand: a genetic and pathologic study using banked human brain tissue. *Neurobiol Aging* **49**, 214 e211-214 e215 (2017).

13. K. L. Williams *et al.*, UBQLN2/ubiquilin 2 mutation and pathology in familial amyotrophic lateral sclerosis. *Neurobiol Aging* **33**, 2527 e2523-2510 (2012).

Supplemental Figures

Fig S1. Confocal microscopy showing the extent of p62 colocalization with UBQLN2 in different regions of the brain of mice at various ages. (A) Confocal microscopy (1x and corresponding 5x zoomed) of the individual and merged images for UBQLN2, p62 and DAPI staining of the dentate gyrus of the hippocampus for the three mouse genotypes at 12 months of age. (B) Images of similar staining in the dentate gyrus, CA1 and cortex regions of the brain in P497S mice at different ages. Panels A (o) and B (d) are the same. Bar sizes shown for this and subsequent images.

Fig S2 Confocal microscopy showing the extent of p62 colocalization with UBQLN2 in the SC of mice at various ages. (A) Confocal microscopy (1x and corresponding 2x zoomed) of individual and merged images for UBQLN2, p62 and DAPI staining in the ventral horn of the SC for the three mouse genotypes at 12 months of age. (B) Similar staining of sections from the SC in P497S animals at 6 and 12 months of age. (C) Confocal microscopy showing colocalization of p62 and UBQLN2 (arrows) within a motor neuron of the SC in a P497S mouse at 12 months of age. Note, the Non-Tg and WT-356 mice do not display similar inclusions.

Fig S3. Confocal microscopy showing lack of colocalization of LC3 with UBQLN2 and/or p62 inclusions in P497S mice. (A, B) Confocal microscopy of LC3A/B staining (Cell signaling antibody) and UBQLN2 in the dentate gyrus (A) and spinal cord (B) of 12-

month-old mice with the genotypes shown. Note lack of colocalization of LC3A/B with the UBQLN2 inclusions in P497S mice.

Fig S4. Lack of colocalization of LC3 with p62 inclusions in P497S mice. (A) Confocal microscopy showing lack of colocalization of p62 and LC3B (Cell Signaling (left set) and abcam (right set) antibodies) in the dentate gryus region of the hippocampus in a 12-month-old P497S animal.

Fig S5. Lack of colocalization of LAMP1 with UBQLN2 and p62 inclusions in P497S mice. (A) Confocal microscopy (1x and 5x zoomed) images of the individual and merged images of the dentate gyrus region of the hippocampus for the three mouse genotypes at 12-months of age. Note excellent colocalization of LAMP1 with p62 and UBQLN2 in both the Non-Tg and WT UBQLN2 animals but not P497S animals (white arrows). However, LAMP1 localizes in separate inclusions (yellow arrows) compared to the UBQLN2 and p62 inclusions in the mutant P497S animal.

Fig S6. UBQLN2 inclusions in human *UBQLN2* cases are positive for p62 staining. (A) Confocal images of the molecular layer (ML), dentate gyrus (DG) and polymorphic layer (PML) brain region (large images) of three different human *UBQLN2* patients carrying either the P497H, P506S or T481I mutations for the different stains shown in color. Zoomed images demonstrate colocalization between UBQLN2 inclusions (green) and p62 (red) in the ML in all three cases. Bar sizes shown. (B) Confocal images of UBQLN2,

p62 and LAMP1 staining in the P506S case, showing lack of colocalization of LAMP1 (white arrows) with the other two proteins (arrow head). Bar 25 μm.

Fig S7. Alteration of autophagic proteins in UBQLN2 KO NSC34 cells. (A) Immunoblots of three independent lysates from the parental NSC34 line and CRISPR/cas9 UBQLN2 KO20 and KO69 lines for the proteins shown. Detection of the different UBQLN isoforms (2nd panel) with an antibody that detects all UBQLNs. (B) Quantification of total UBQLN protein expression in the parental and KO NSC34 lines. (C) Immunoblot of three independent cell lysates from the parental HeLa and NSC34 cell lines together with 2-fold dilutions of known amounts of GST-UBQLN2 fusion protein blotted with an antibody specific for UBQLN2. (D) The graph shows the quantification of UBQLN2 expression in the lines.

Fig S8. Quantification of p62 expression in normal HeLa and UBQLN2 knockout cell lines. (A) Real-time quantitative PCR measurement of p62 mRNA in the three different HeLa cell lines. Although the two UBQLN2 KO lines had slightly increased p62 expression compared to the parental line, the difference was not significant. (B) Immunofluorescence staining of normal HeLa (a and b) and UBQLN2 KO8 (c and d) cell lines. Note p62 forms inclusions in the UBQLN2 KO8 cells. (C) Quantification of the intensity of p62 fluorescence staining of 10 different cells shown in B suggests little variation between the two cell lines. (D) Quantification showing UBQLN2 KO8 cells have a large increase in inclusions (between 0.3 and 2 μm in size) compared to the parental HeLa line.

Fig S9. Inactivation of UBQLN2 in HeLa cells reduces autophagic flux. (A-H) HeLa and the UBQLN2 KO8 (A-D) and KO12 (E-H) cell lines were cultured either in DMEM medium with Glucose (Glu) or shifted to DMEM medium lacking glucose (-Glu) (A, B, E and F) or to plain EBSS buffer (C, D, G and H) for different lengths of time (0, 2 and 4 hrs) with or without Bafilomycin A1 (Baf A1). Protein lysates were prepared from the cultures and immunoblotted for LC3, p62 and for actin, as a loading control. The graphs on the right-hand side show the changes in LC3II for each set of immunoblots after correcting for actin loading and normalization to the HeLa parental line grown in DMEM without any treatment.

Fig S10. Venus reporter constructs used to track maturation of UBQLN2-containing autophagosomes into autolysosomes. (A) Schematic constructs of the fluorescent reporters used to study the fate of UBQLN2 in cells. 1. Traditional GFP-mCherry-LC3B reporter. 2-5. NVenus and CVenus expression constructs and subsequent derivatives of them. The fluorescent signals following reconstitution of Venus fluorescence (=) is shown to the right for each set. (B) Immunoblots of HeLa cell lysates following transfection with the two different Venus reporter constructs shown with antibodies to either LC3B or GFP. The arrow heads indicate the position of the full-length proteins that correspond to the correct predicted size for each fusion-construct. (C) Immunoblots of HeLa cells transfected with the NVenus-tagged WT and ALS/FTD mutant UBQLN2 constructs using an anti-HA antibody, verifying the correct fusion proteins were made for each construct. (D) Staining of endogenous UBQLN2 and LC3B in HeLa cells.

Arrows show colocalization of the staining in puncta. (E) Fluorescent (YFP) images of HeLa cells transfected with N (a) or CVenus (b) alone or together (c). (F) Cells transfected with NVenus-UBQLN2 WT and CVenus and counterstained for LC3B (a-d). (G) Images of HeLa cells transfected with either CVenus-mCherry-LC3B alone (a-d). Note lack of Venus fluorescence without cotransfection with NVenus-UBQLN2.

Fig S11. Disappearance of autophagic markers during autophagosome to autolysosome conversion. (A-C) Images of cells with reconstituted Venus fluorescence after transfection of either WT or the P525S UBQLN2 reporters and stained (Alexa 405 secondary antibody) for p62 (A), ubiquitin (Ub) (B), or UBQLN2 (C) itself. Note most yellow puncta that demarcate autophagosomes contain all three markers (white arrows), whereas most red puncta that demarcate autolysosomes lack the markers (yellow arrows). The number and percentage of red or yellow puncta that stained positive were: for p62 staining of cells transfected with WT-UBQLN2, 0/7 of the red puncta were positive = 0%, whereas 17/17 of the yellow puncta were positive = 100% (very small puncta were excluded as the p62 staining was difficult to evaluate); for p62 staining of cells transfected with the P525S UBQLN2 mutant, 0/4 of the red puncta were p62 positive = 0% and 18/18 of the yellow puncta were p62 positive = 100%. For Ub staining of cells transfected with WT-UBQLN2, 0/19 red puncta were Ub positive = 0% and 16/24 of the yellow puncta were Ub positive 66%, whereas for the P525S mutant 0/19 of the red puncta were Ub positive = 0% and 14/15 yellow puncta were Ub positive = 93%. These results are consistent with our idea that the red puncta are autolysosomes which have degraded their contents, whereas the yellow puncta are

autophagosomes that have not acidified and therefore have not degraded their content. (D) Similar to A-C, but this time the fluorescence was quenched before the cells were stained for UBQLN2, LC3A/B and LAMP1. Note LAMP1 staining is detectable in several (white arrows) but not all puncta (yellow arrows), demonstrating key components required for autophagosome maturation can be recruited to UBQLN2-containing puncta.

Fig S12. Autophagosomal-lysosomal dysfunction in HeLa UBQLN2 KO8 cells. (A) Individual and combined images of HeLa (a-d) and KO8 (e-h) cells transfected with the traditional GFP-mCherry-LC3B reporter. (B) Quantification of autophagosome number and acidification in HeLa and KO8 cells. (C) Immunoblots of three independent culture lysates for WIPI2. (D) Quantification of WIPI2 expression for the blots shown in C. (E) Immunofluorescence staining of WIPI2 and LC3A/B in HeLa and KO8 cells cultured in either regular DMEM or after shifting for 4 hr in medium lacking glucose (-Glu). (F) Lysotracker staining of HeLa and KO8 cells. (G) Quantification of Lysotracker staining in the two cell lines. (H) Immunoblots of three independent culture lysates for Cathepsin D (the position of the pro and mature (mat) forms of the protein are shown). (I) Graph showing the calculated ratio of the mature to pro Cathepsin D in the blots shown in H.

Fig S13. Overexpression of ALS/FTD mutant UBQLN2 proteins in HeLa cells inhibits autophagosome acidification. (A) Representative images of the combined YFP, mCherry and DAPI fluorescent signals in normal HeLa cells cotransfected with CVenus-mCherry-LC3B with either WT or ALS mutant NVenus-UBQLN2 constructs. The individual panels for these merged images are shown in Fig S14. (H) Quantification of

autophagosome acidification using the reporter constructs shown in A. Note, autophagosome acidification for the control HeLa cells was done with the traditional GFP-mCherry-LC3 reporter.

Fig S14. Reconstitution of Venus fluorescence using the UBQLN2 reporter constructs to study autophagosome acidification in normal HeLa cells. (a-x) Individual and combined images for each set of constructs shown in Fig S13A.

Fig S15. Reconstitution of Venus fluorescence using the UBQLN2 reporter constructs to study autophagosome acidification in HeLa KO8 cells. (a-x) Individual and combined images for each set of constructs shown in Fig 4A.

Fig S16. Alteration of ATP6v1g1 levels in P497S mutant and UBQLN2 KO mice. (A) Proteomic data showing the Log_2 ratio of change of all subunits detected for the V-ATPase pump between P497S mutant and WT UBQLN2, or Non-Tg mice in the lower lumbar region of the SC and Hippocampus of mice at 2 months of age. (B) Immunoblots of SC lysates from 14 different Non-Tg and P497S mice at 6 months of age. (C) Quantification of changes in protein levels of the two V-ATPase subunits analyzed in B. (D) Immunoblots of brain lysates from 12-month-old Non-Tg and UBQLN2 KO animals for the proteins shown. (E) Quantification of ATP6v1g1 levels in the blots shown in D.

Fig S17. ATP6v1g1 localization in mouse brain. (A) Confocal microscopy of UBQLN2, ATP6v1g1 and DAPI staining of the dentate gyrus in 12-month-old Non-Tg, WT

UBQLN2 Tg and P497S UBQLN2 Tg mice. Note lack of ATP6v1g1 staining of the UBQLN2 inclusions in the P497S animal.

Fig S18. Studies of UBQLN2 interaction and regulation of ATP6v1g1 levels. (A) Turnover of ATP6v1g1 in HeLa and KO8 cells analyzed by a cycloheximide (CHX) chase experiment. (B) Quantification of the turnover of ATP6v1g1 in HeLa and KO8 cells. The exponential trend line of the turnover for each cell line is shown by the dashed lines. (C) Effects of proteasome and autophagy inhibition on the UBQLN2-induced induction of ATP6v1g1 biogenesis. Immunoblots of parallel cultures transfected with the constructs shown and which were either left untreated or treated with MG132 or Bafilomycin A1 for 4 hours. (D) Quantification of ATP6v1g1 levels relative to the control culture that was transfected with 1 μg of ATP6v1g1 alone. Note that proteasome inhibition elevates ATP6v1g1 levels beyond those found in the control cultures. (E) GST-pulldown assay showing a Coomassie stained gel of the purified recombinant proteins used in the assay and the resulting pulldown results. (F) Quantification of ATP6v1g1-His pulled down relative to the amount of GST protein.

Fig S19. Knockdown of ATP6v1g1 reduces autophagosome acidification. (A) Images of the different fluorescent panels that were used to construct the merged images shown in Fig 6G that demonstrates knockdown of ATP6v1g1 impedes autophagosome acidification as evident by accumulation of more yellow puncta.

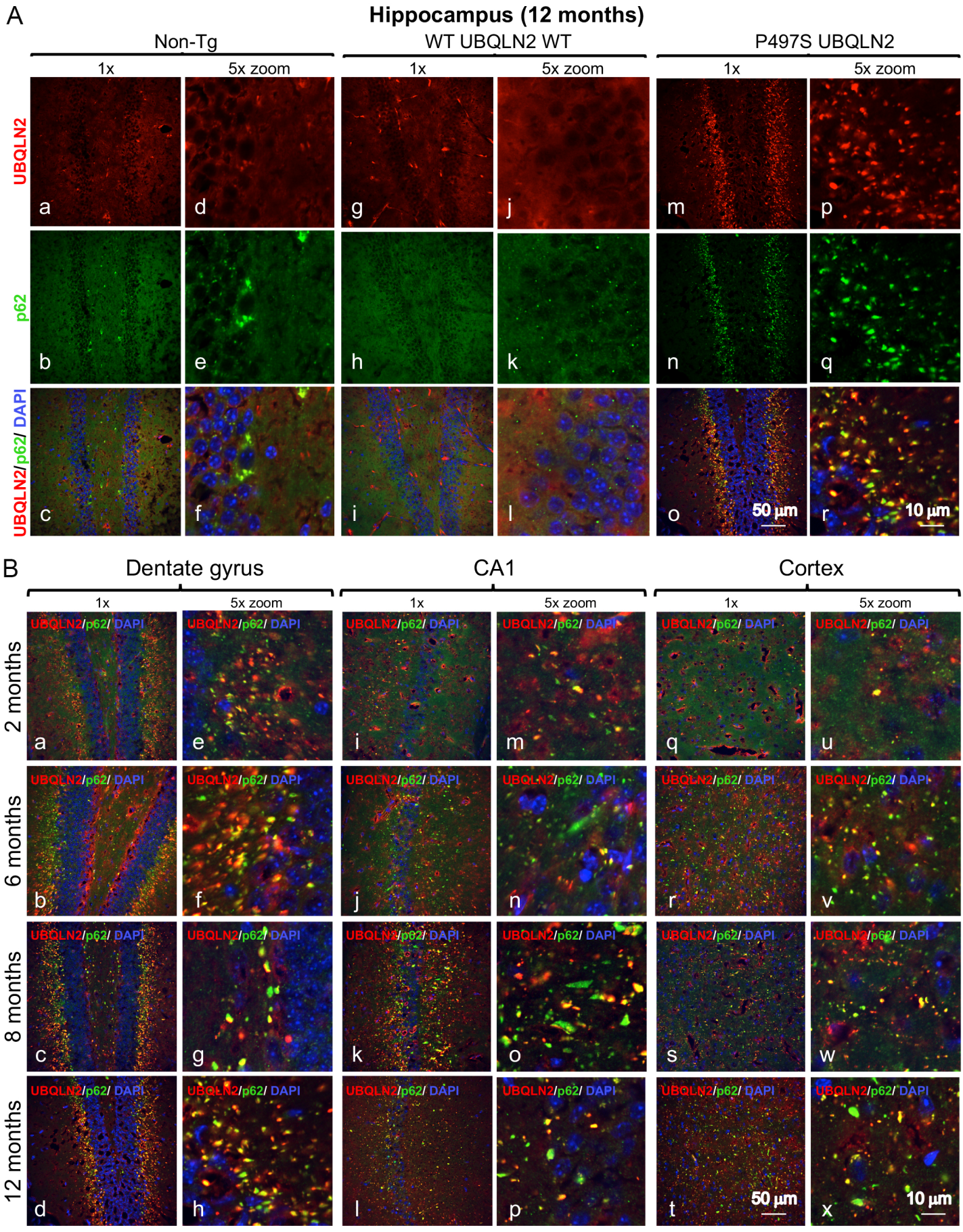
A
Hippocampus (12 months)
Non-Tg
WT UBQLN2 WT
P497S UBQLN2
1x
5x zoom
UBQLN2
p62
UBQLN2/p62/ DAPI
a
b
c
d
e
f
g
h
i
j
k
l
m
n
o
p
q
r
50 µm
10 µm
B
Dentate gyrus
CA1
Cortex
2 months
6 months
8 months
12 months
UBQLN2/p62/ DAPI
a
b
c
d
e
f
g
h
i
j
k
l
m
n
o
p
q
r
s
t
u
v
w
x
50 µm
10 µm

Fig S1

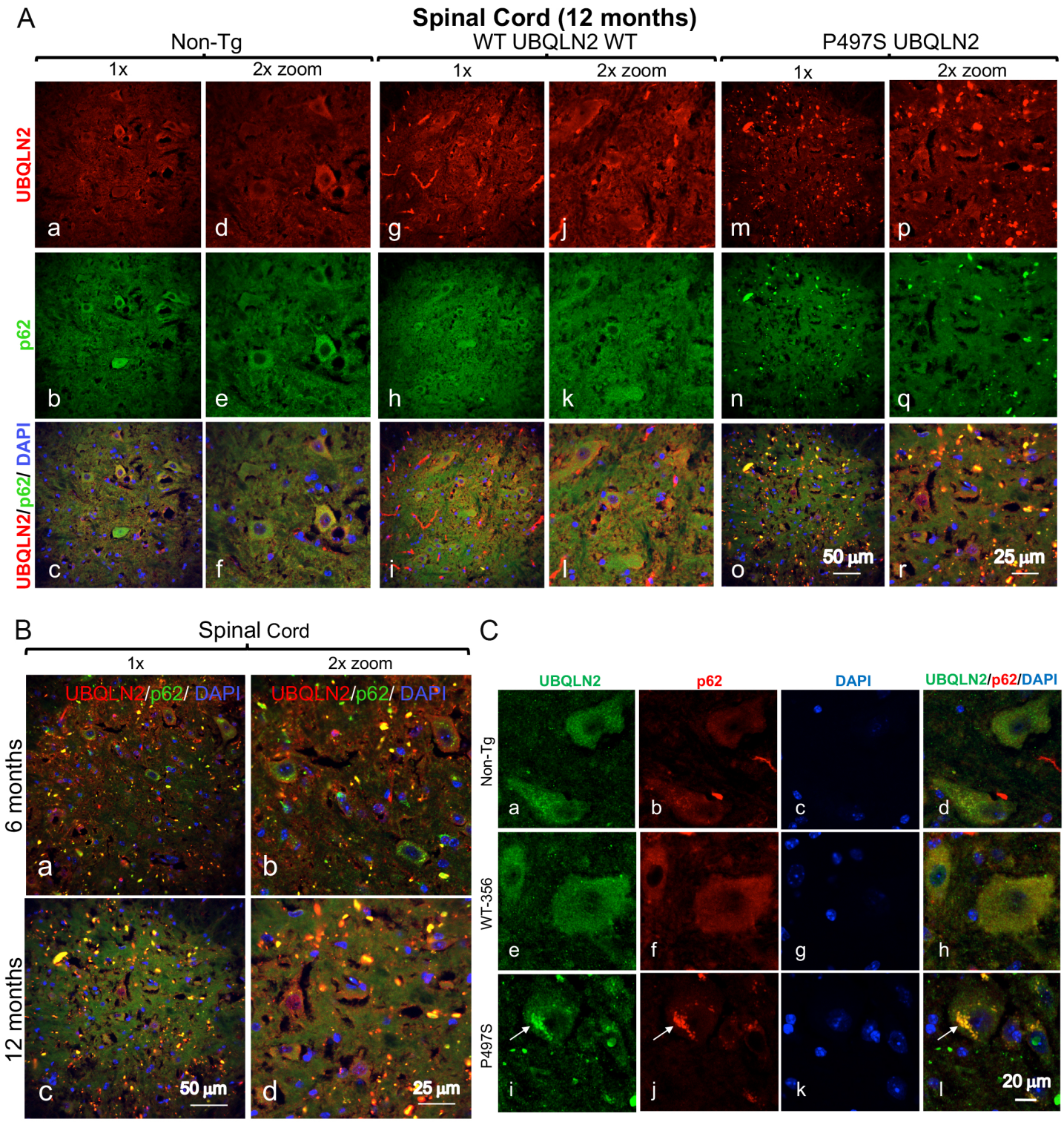
A
Spinal Cord (12 months)
Non-Tg
WT UBQLN2 WT
P497S UBQLN2
1x
2x zoom
1x
2x zoom
1x
2x zoom
UBQLN2
p62
UBQLN2/p62/ DAPI
a
b
c
d
e
f
g
h
i
j
k
l
m
n
o
p
q
r
50 µm
25 µm
B
Spinal Cord
1x
2x zoom
6 months
12 months
UBQLN2/p62/ DAPI
UBQLN2/p62/ DAPI
a
b
c
d
50 µm
25 µm
C
UBQLN2
p62
DAPI
UBQLN2/p62/DAPI
Non-Tg
WT-356
P497S
a
b
c
d
e
f
g
h
i
j
k
l
20 µm

Fig S2

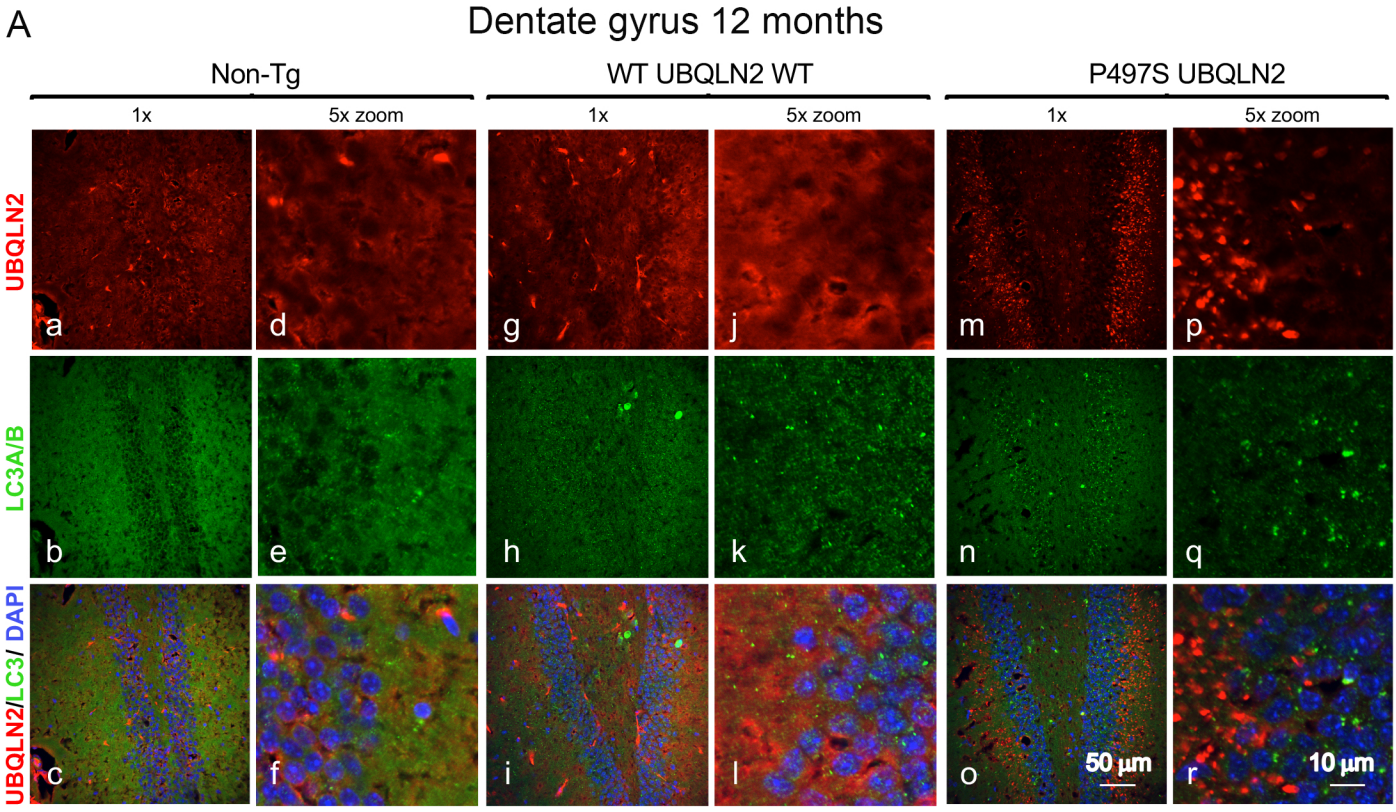
A
Dentate gyrus 12 months
Non-Tg
WT UBQLN2 WT
P497S UBQLN2
1x
5x zoom
UBQLN2
LC3A/B
UBQLN2/LC3/ DAPI
a
b
c
d
e
f
g
h
i
j
k
l
m
n
o
p
q
r
50 µm
10 µm

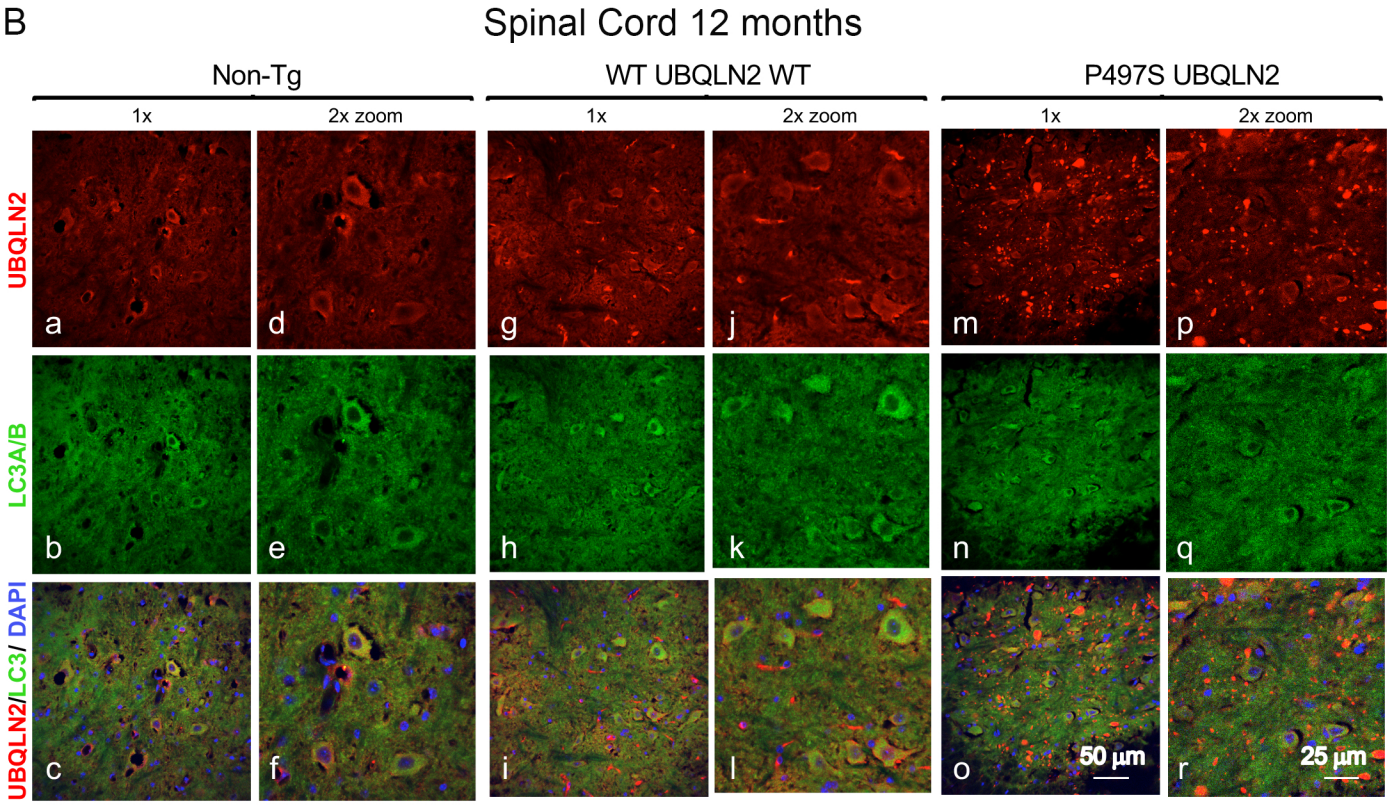
B
Spinal Cord 12 months
Non-Tg
WT UBQLN2 WT
P497S UBQLN2
1x
2x zoom
UBQLN2
LC3A/B
UBQLN2/LC3/ DAPI
a
b
c
d
e
f
g
h
i
j
k
l
m
n
o
p
q
r
50 µm
25 µm

Fig S3

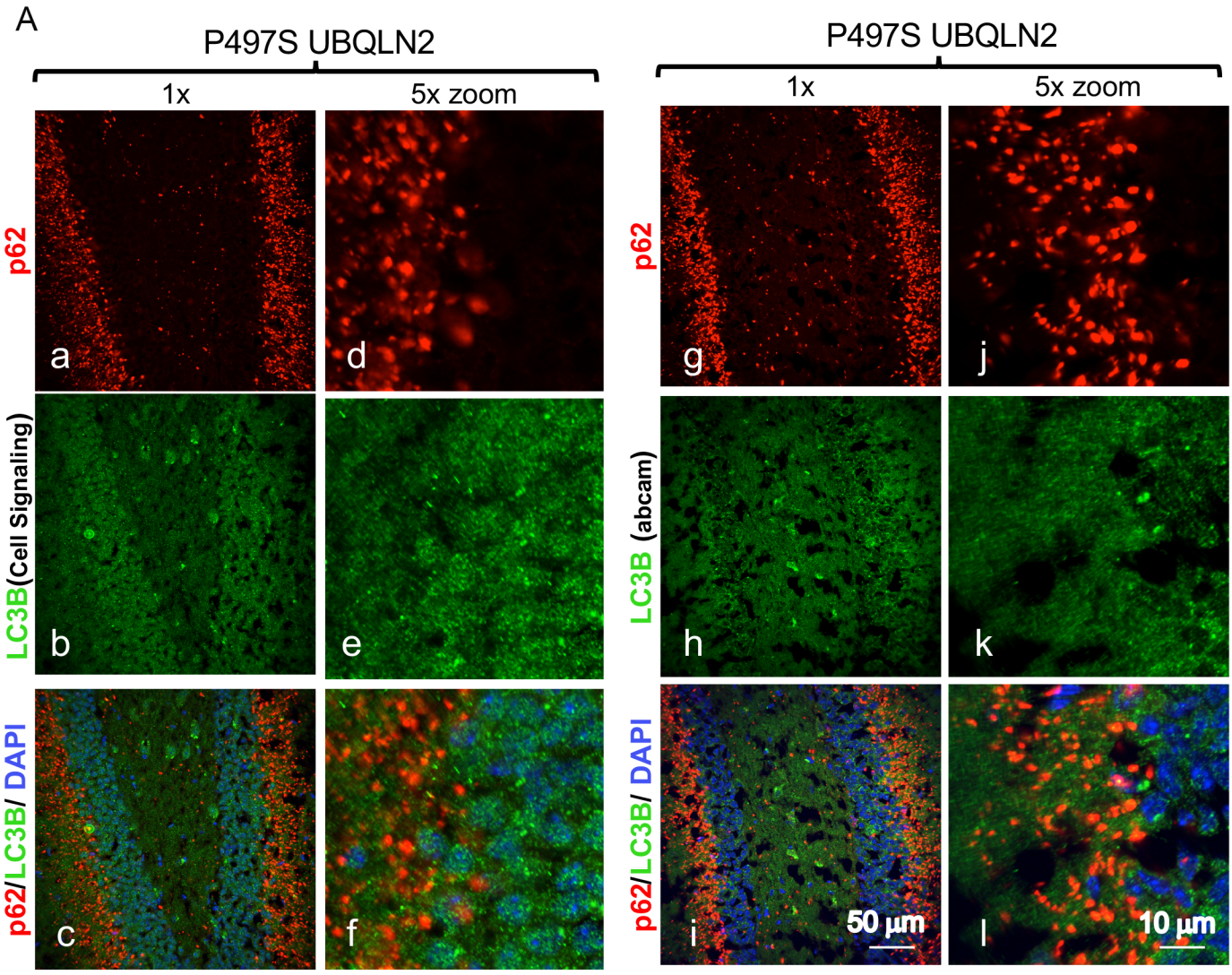
A
P497S UBQLN2
1x
5x zoom
P497S UBQLN2
1x
5x zoom
p62
LC3B (Cell Signaling)
p62/LC3B/ DAPI
LC3B (abcam)
p62/LC3B/ DAPI
a
b
c
d
e
f
g
h
i
j
k
l
50 µm
10 µm

Fig S4

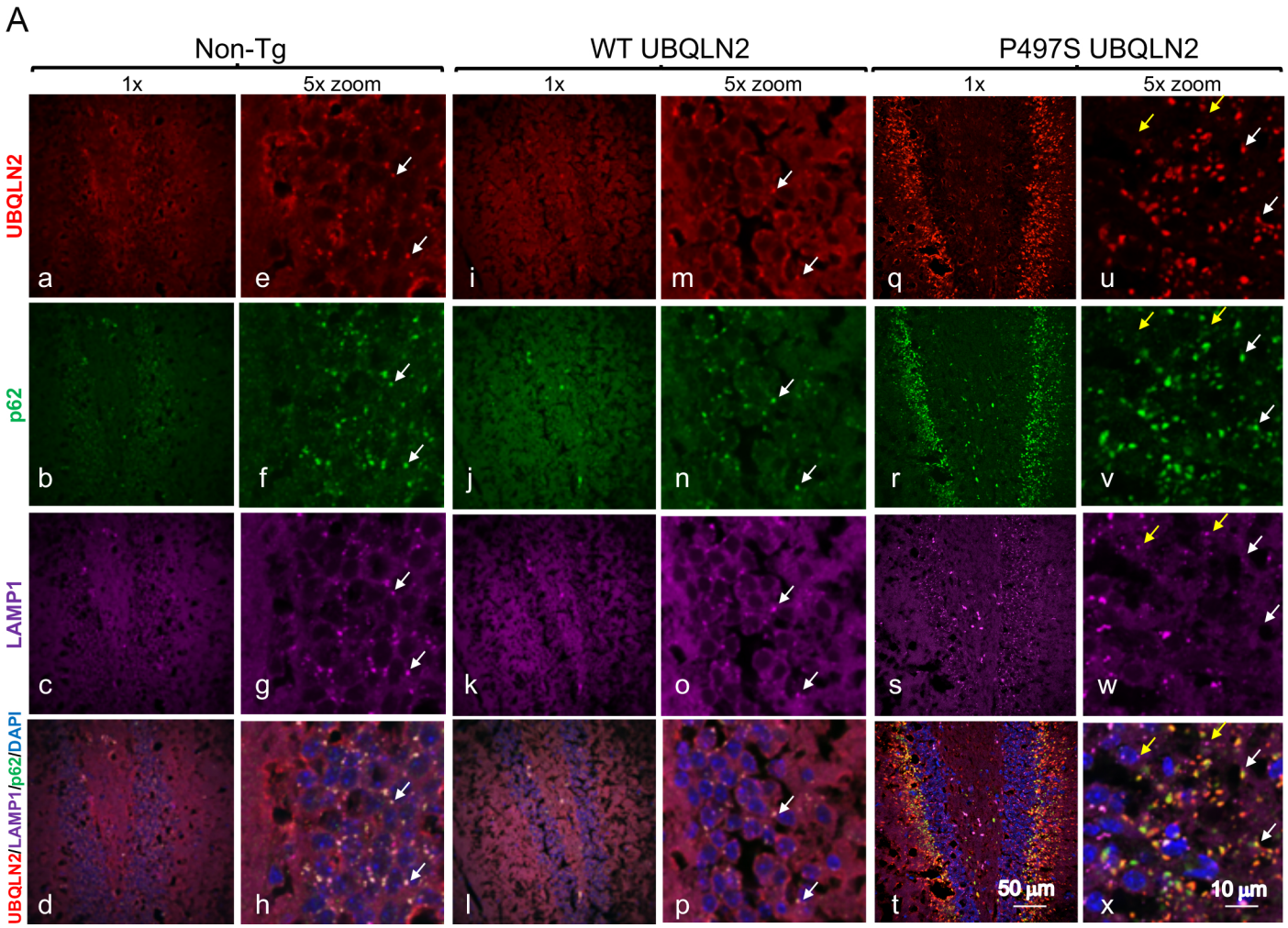
A
Non-Tg
WT UBQLN2
P497S UBQLN2
1x
5x zoom
1x
5x zoom
1x
5x zoom
UBQLN2
p62
LAMP1
UBQLN2/LAMP1/p62/DAPI
a
e
i
m
q
u
b
f
j
n
r
v
c
g
k
o
s
w
d
h
l
p
t
x
50 µm
10 µm

Fig S5

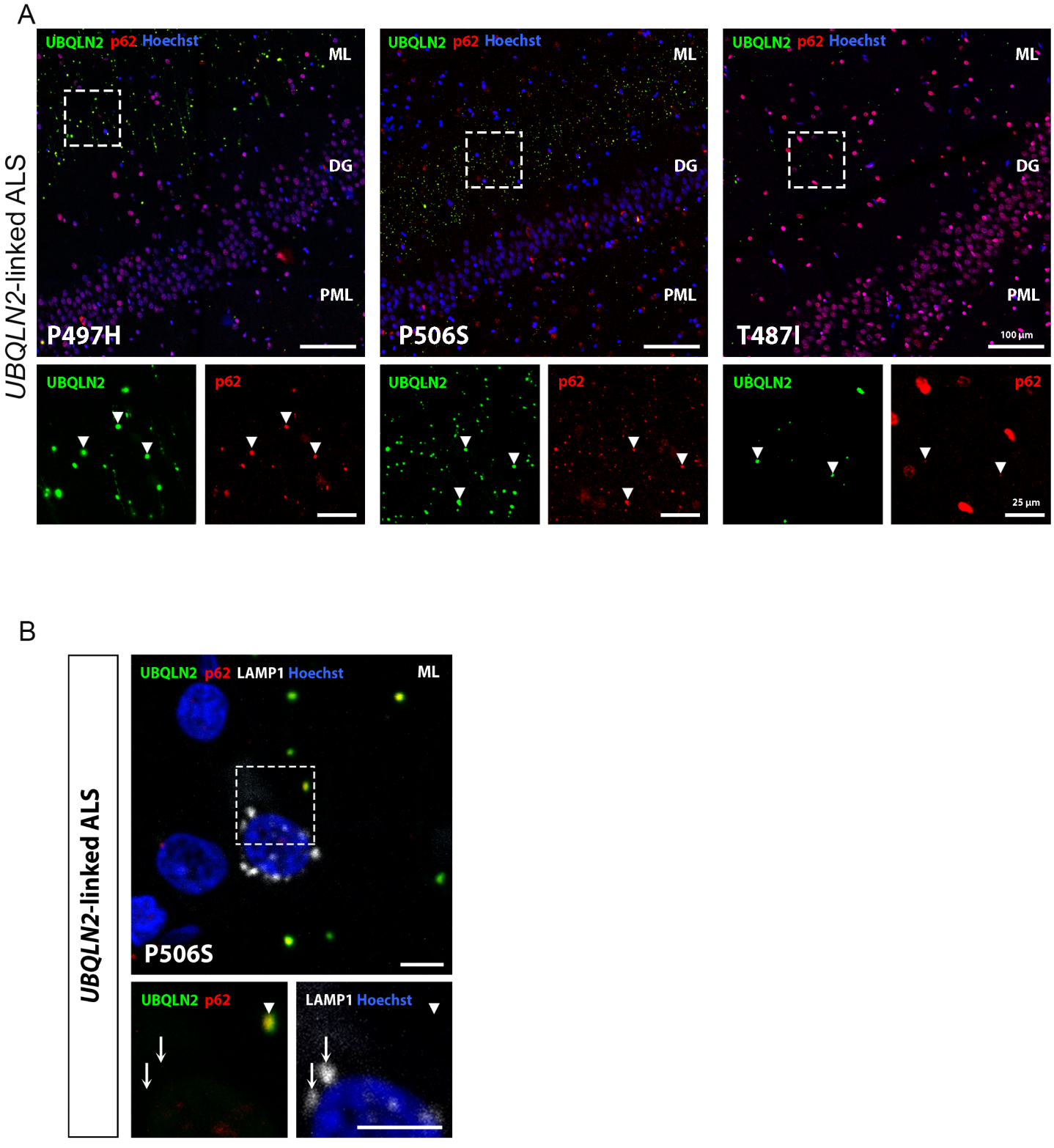
A
UBQLN2-linked ALS
UBQLN2 p62 Hoechst
ML
DG
PML
P497H
P506S
T487I
100 µm
UBQLN2
p62
25 µm
B
UBQLN2-linked ALS
UBQLN2 p62 LAMP1 Hoechst
ML
P506S
UBQLN2 p62
LAMP1 Hoechst

Fig S6

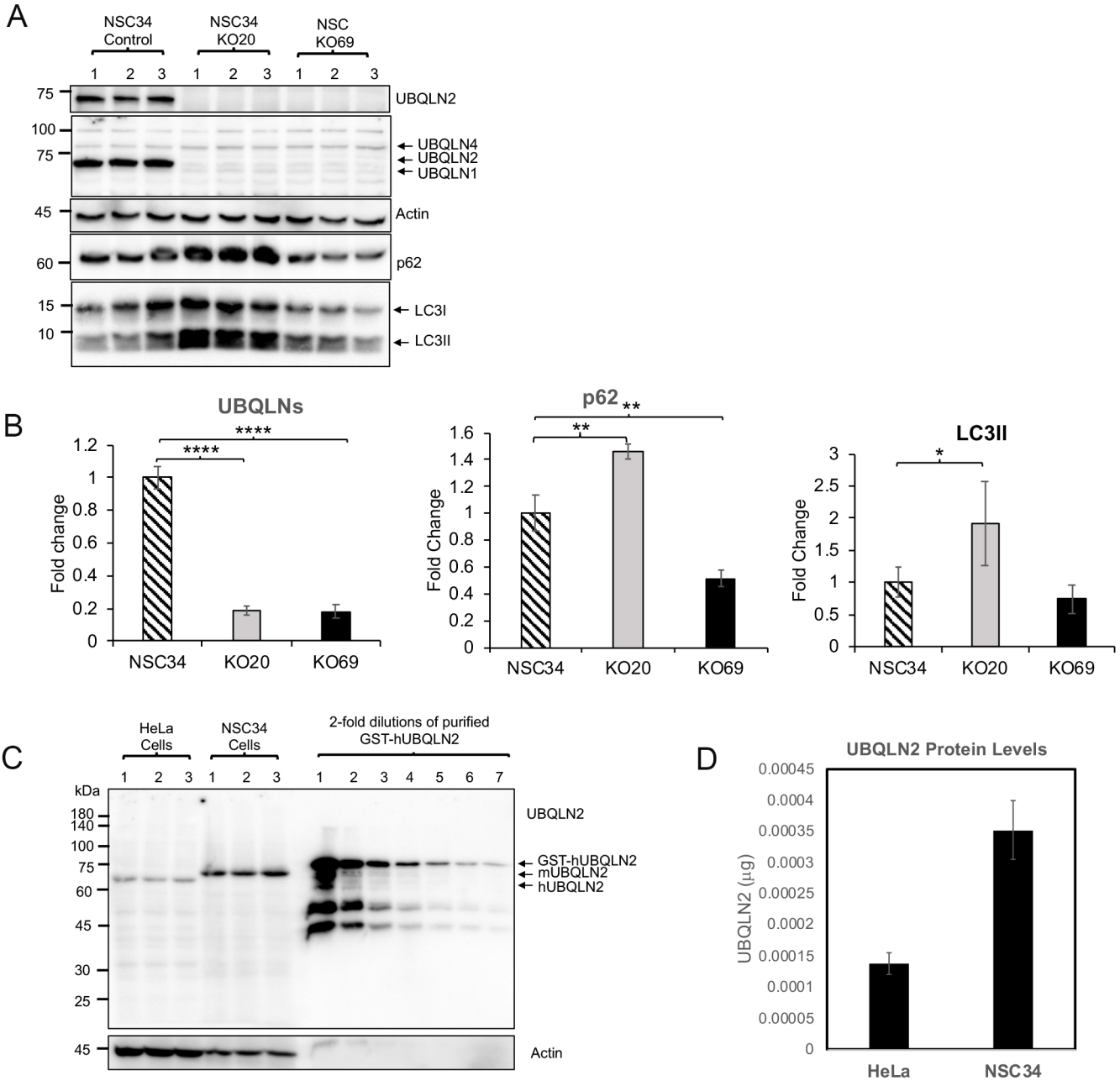
A
NSC34 Control
NSC34 KO20
NSC KO69
1 2 3 1 2 3 1 2 3
75
UBQLN2
100
75
UBQLN4
UBQLN2
UBQLN1
45
Actin
60
p62
15
LC3I
10
LC3II
B
UBQLNs
****
****
Fold change
1.2
1
0.8
0.6
0.4
0.2
0
NSC34
KO20
KO69
p62
**
**
Fold Change
1.6
1.4
1.2
1
0.8
0.6
0.4
0.2
0
NSC34
KO20
KO69
LC3II
*
Fold Change
3
2.5
2
1.5
1
0.5
0
NSC34
KO20
KO69
C
HeLa Cells
NSC34 Cells
2-fold dilutions of purified GST-hUBQLN2
1 2 3 1 2 3 1 2 3 4 5 6 7
kDa
180
140
100
75
60
45
30
25
UBQLN2
GST-hUBQLN2
mUBQLN2
hUBQLN2
45
Actin
D
UBQLN2 Protein Levels
UBQLN2 (µg)
0.00045
0.0004
0.00035
0.0003
0.00025
0.0002
0.00015
0.0001
0.00005
0
HeLa
NSC34

Fig S7

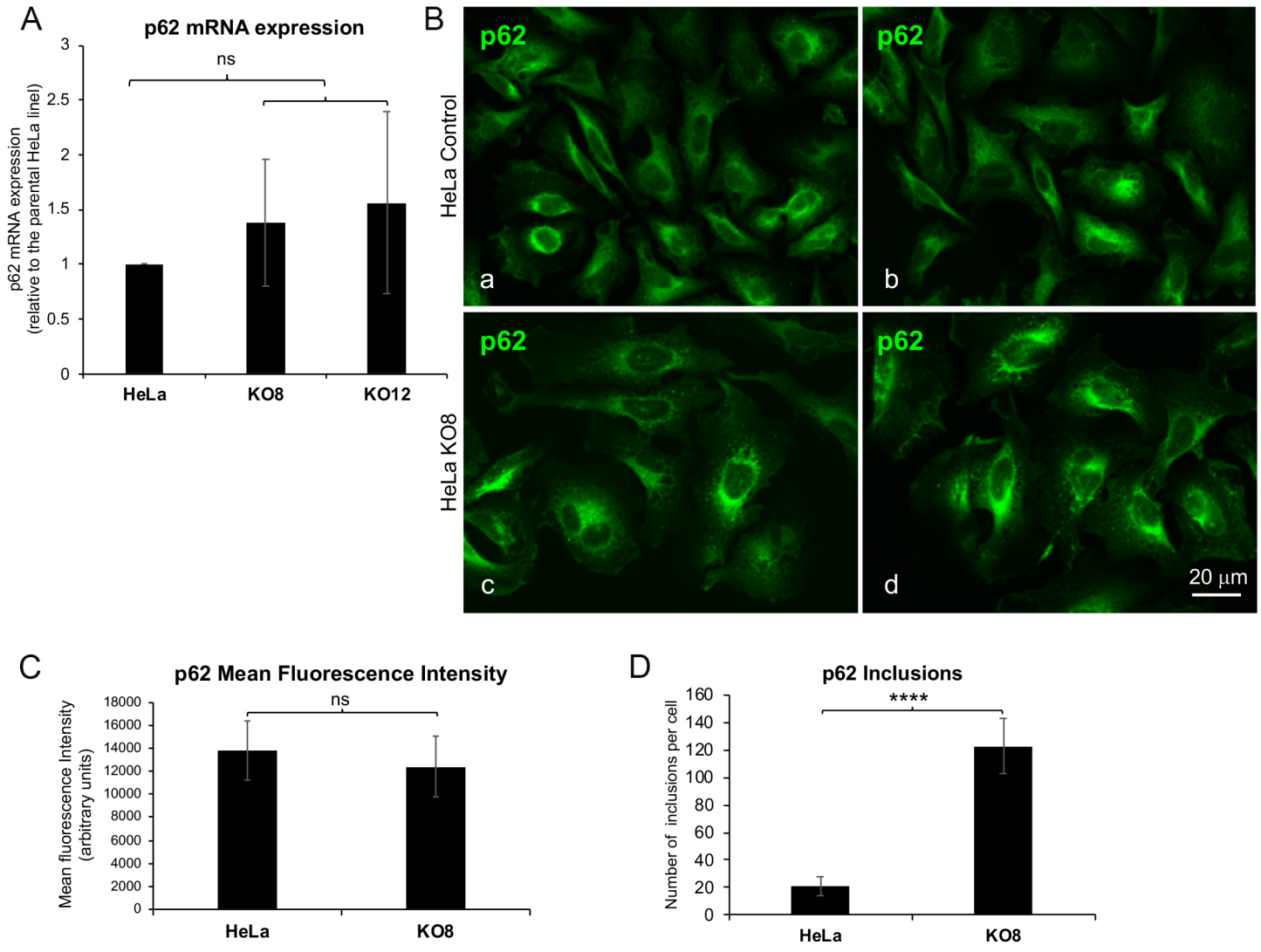
A
p62 mRNA expression
ns
p62 mRNA expression
(relative to the parental HeLa line)
3
2.5
2
1.5
1
0.5
0
HeLa
KO8
KO12
B
p62
HeLa Control
HeLa KO8
a
b
c
d
20 μm
C
p62 Mean Fluorescence Intensity
ns
Mean fluorescence Intensity
(arbitrary units)
18000
16000
14000
12000
10000
8000
6000
4000
2000
0
HeLa
KO8
D
p62 Inclusions
****
Number of inclusions per cell
160
140
120
100
80
60
40
20
0
HeLa
KO8

Fig S8

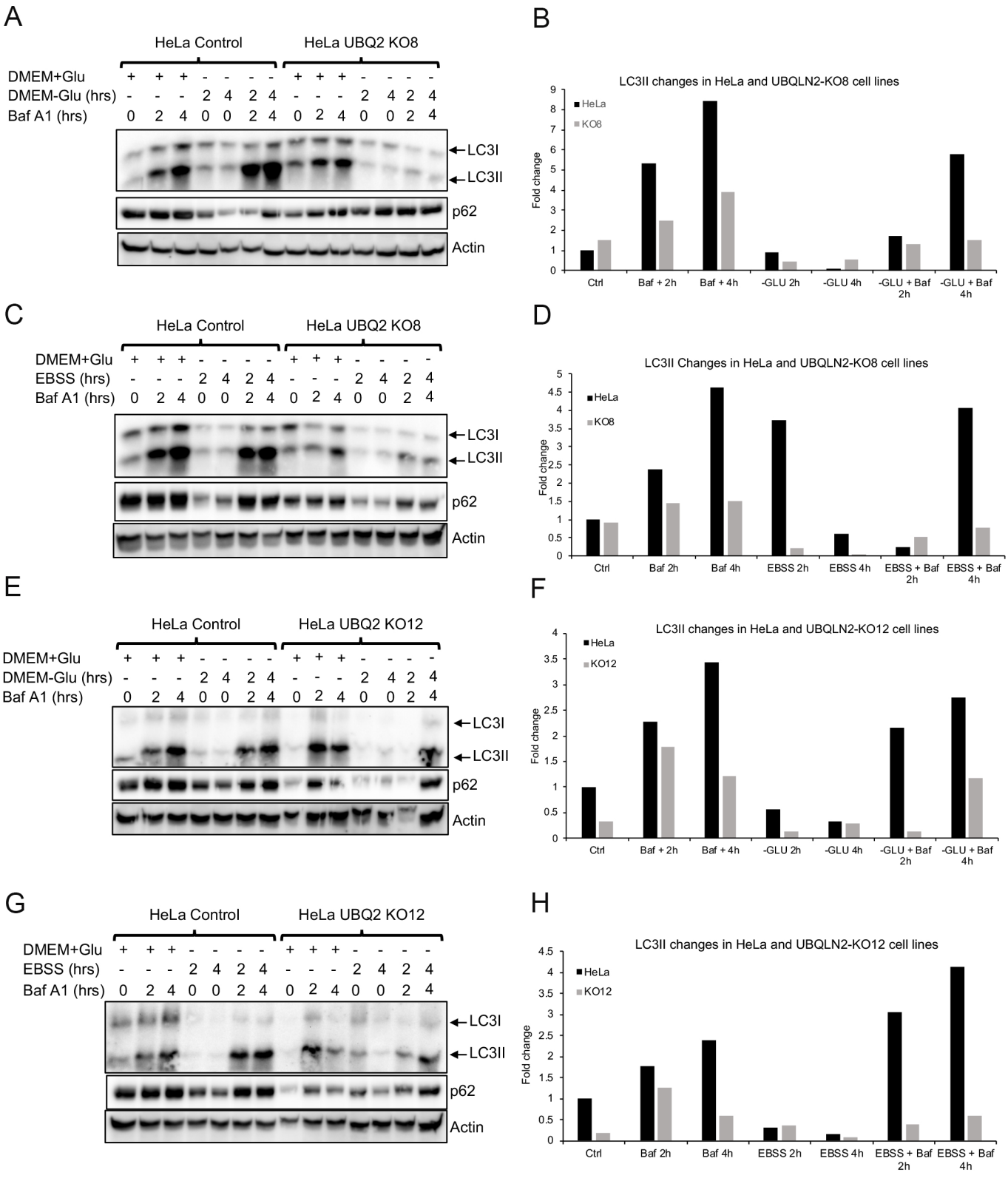
A
HeLa Control
HeLa UBQ2 KO8
DMEM+Glu
DMEM-Glu (hrs)
Baf A1 (hrs)
LC3I
LC3II
p62
Actin
B
LC3II changes in HeLa and UBQLN2-KO8 cell lines
HeLa
KO8
Fold change
Ctrl
Baf + 2h
Baf + 4h
-GLU 2h
-GLU 4h
-GLU + Baf 2h
-GLU + Baf 4h
C
HeLa Control
HeLa UBQ2 KO8
DMEM+Glu
EBSS (hrs)
Baf A1 (hrs)
LC3I
LC3II
p62
Actin
D
LC3II Changes in HeLa and UBQLN2-KO8 cell lines
HeLa
KO8
Fold change
Ctrl
Baf 2h
Baf 4h
EBSS 2h
EBSS 4h
EBSS + Baf 2h
EBSS + Baf 4h
E
HeLa Control
HeLa UBQ2 KO12
DMEM+Glu
DMEM-Glu (hrs)
Baf A1 (hrs)
LC3I
LC3II
p62
Actin
F
LC3II changes in HeLa and UBQLN2-KO12 cell lines
HeLa
KO12
Fold change
Ctrl
Baf + 2h
Baf + 4h
-GLU 2h
-GLU 4h
-GLU + Baf 2h
-GLU + Baf 4h
G
HeLa Control
HeLa UBQ2 KO12
DMEM+Glu
EBSS (hrs)
Baf A1 (hrs)
LC3I
LC3II
p62
Actin
H
LC3II changes in HeLa and UBQLN2-KO12 cell lines
HeLa
KO12
Fold change
Ctrl
Baf 2h
Baf 4h
EBSS 2h
EBSS 4h
EBSS + Baf 2h
EBSS + Baf 4h

Fig S9

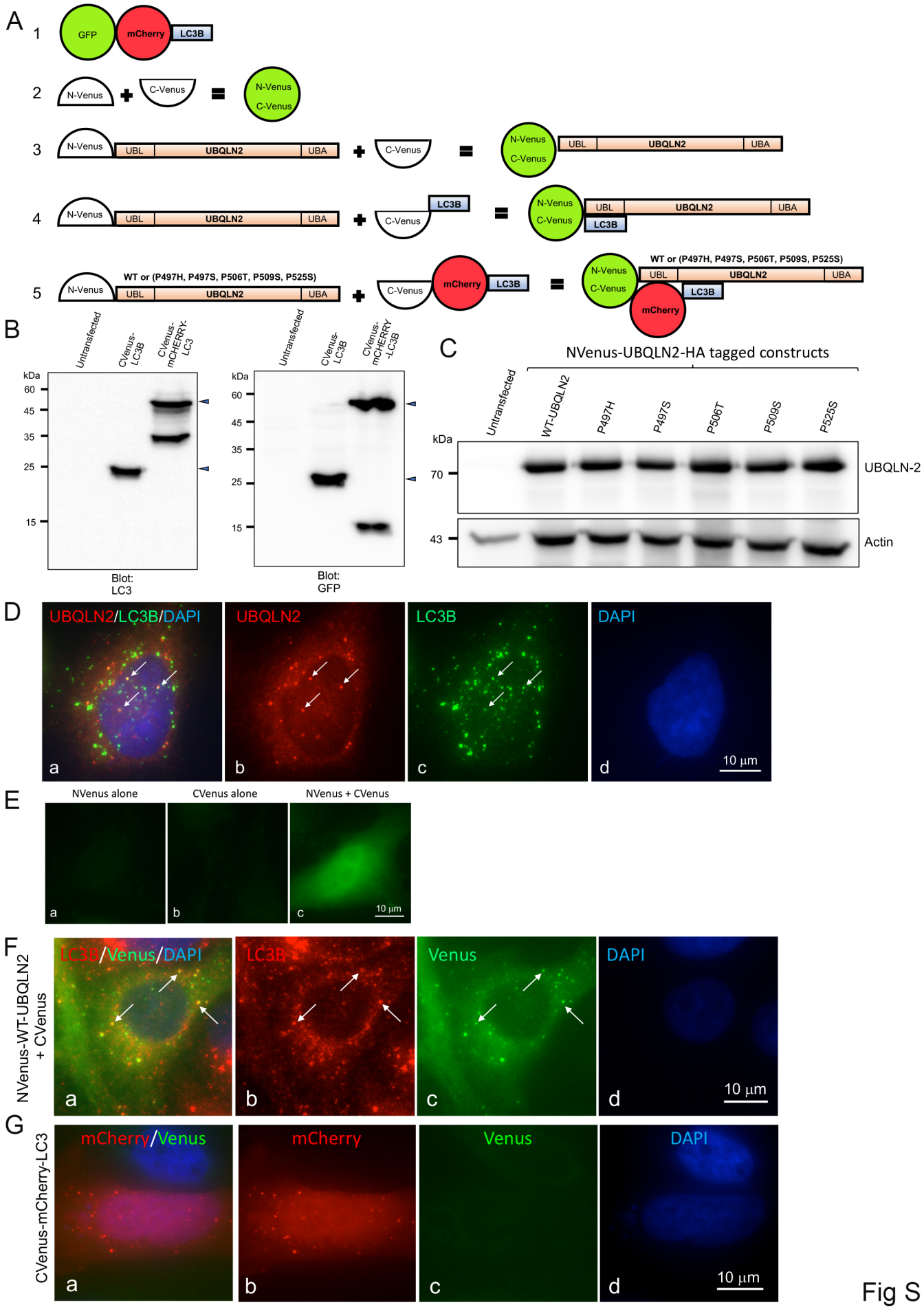
A
1
GFP
mCherry
LC3B
2
N-Venus
C-Venus
N-Venus
C-Venus
3
N-Venus
UBL
UBQLN2
UBA
C-Venus
N-Venus
C-Venus
UBL
UBQLN2
UBA
4
N-Venus
UBL
UBQLN2
UBA
C-Venus
LC3B
N-Venus
C-Venus
UBL
UBQLN2
UBA
LC3B
5
N-Venus
WT or (P497H, P497S, P506T, P509S, P525S)
UBL
UBQLN2
UBA
C-Venus
mCherry
LC3B
N-Venus
C-Venus
WT or (P497H, P497S, P506T, P509S, P525S)
UBL
UBQLN2
UBA
LC3B
mCherry
B
Untransfected
CVenus-LC3B
CVenus-mCHERRY-LC3
kDa
60
45
35
25
15
Blot: LC3
Untransfected
CVenus-LC3B
CVenus-mCHERRY-LC3B
kDa
60
45
35
25
15
Blot: GFP
C
NVenus-UBQLN2-HA tagged constructs
Untransfected
WT-UBQLN2
P497H
P497S
P506T
P509S
P525S
kDa
70
UBQLN-2
43
Actin
D
UBQLN2/LC3B/DAPI
UBQLN2
LC3B
DAPI
a
b
c
d
10 µm
E
NVenus alone
CVenus alone
NVenus + CVenus
a
b
c
10 µm
F
NVenus-WT-UBQLN2 + CVenus
LC3B/Venus/DAPI
LC3B
Venus
DAPI
a
b
c
d
10 µm
G
CVenus-mCherry-LC3
mCherry/Venus
mCherry
Venus
DAPI
a
b
c
d
10 µm

Fig S10

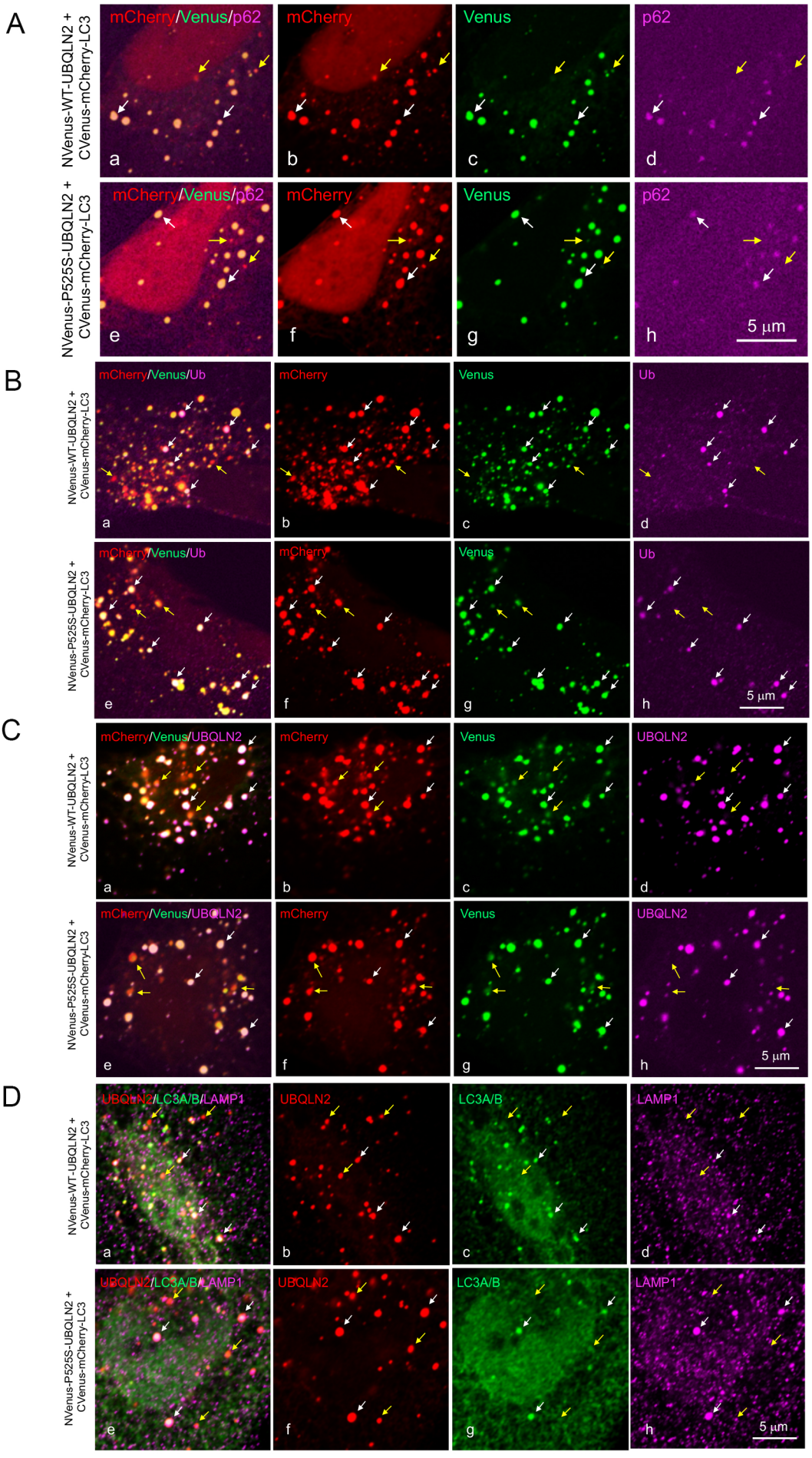
A
NVenus-WT-UBQLN2 + CVenus-mCherry-LC3
NVenus-P525S-UBQLN2 + CVenus-mCherry-LC3
mCherry/Venus/p62
mCherry
Venus
p62
a
b
c
d
e
f
g
h
5 μm
B
mCherry/Venus/Ub
Ub
C
mCherry/Venus/UBQLN2
UBQLN2
D
UBQLN2/LC3A/B/LAMP1
LC3A/B
LAMP1

Fig S11

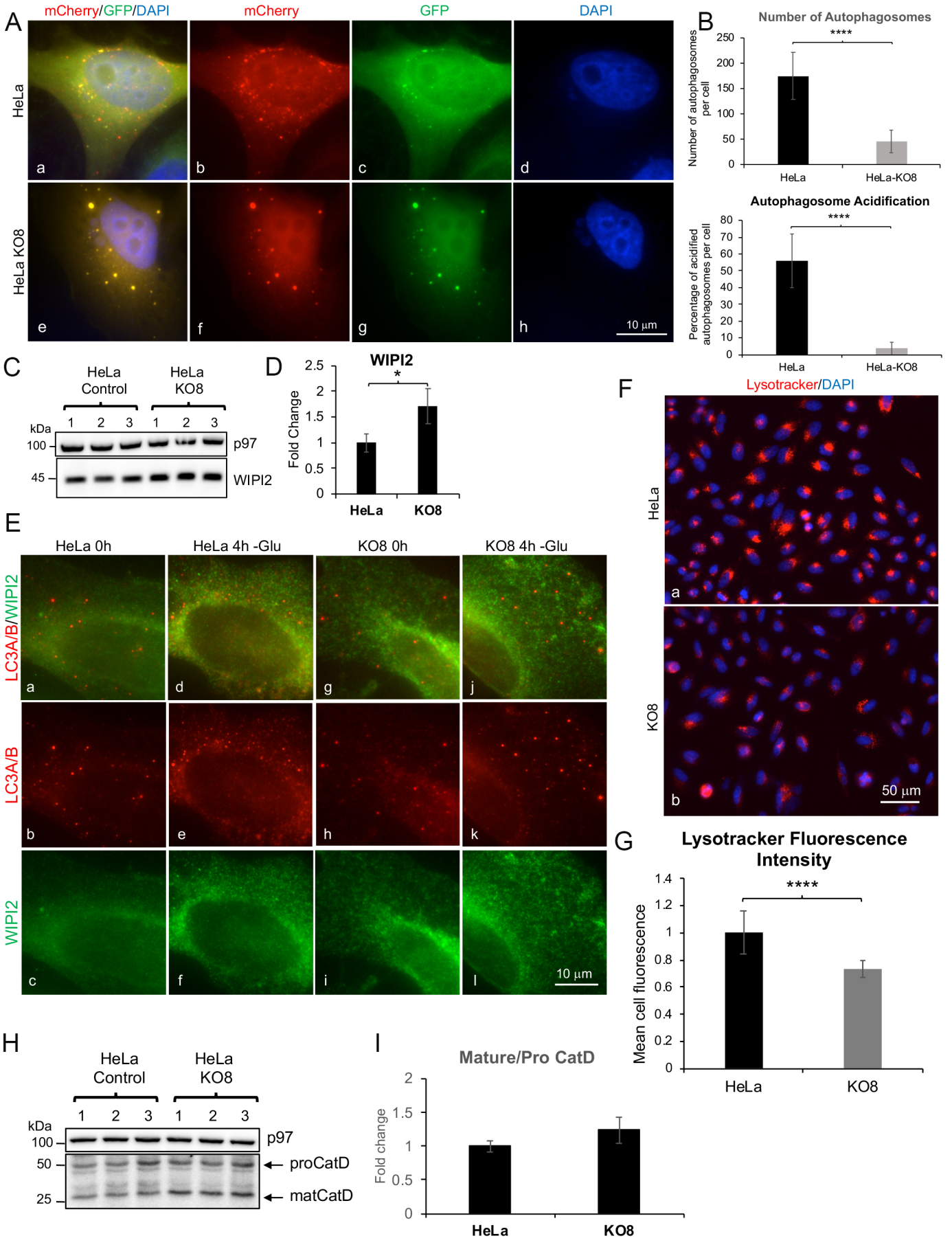
A
mCherry/GFP/DAPI
mCherry
GFP
DAPI
HeLa
HeLa KO8
a
b
c
d
e
f
g
h
10 μm
B
Number of Autophagosomes
****
Number of autophagosomes per cell
250
200
150
100
50
0
HeLa
HeLa-KO8
Autophagosome Acidification
****
Percentage of acidified autophagosomes per cell
80
70
60
50
40
30
20
10
0
HeLa
HeLa-KO8
C
HeLa Control
HeLa KO8
1 2 3 1 2 3
kDa
100
45
p97
WIPI2
D
WIPI2
*
Fold Change
2.5
2
1.5
1
0.5
0
HeLa
KO8
E
HeLa 0h
HeLa 4h -Glu
KO8 0h
KO8 4h -Glu
LC3A/B/WIPI2
LC3A/B
WIPI2
a
d
g
j
b
e
h
k
c
f
i
l
10 μm
F
Lysotracker/DAPI
HeLa
KO8
a
b
50 μm
G
Lysotracker Fluorescence Intensity
****
Mean cell fluorescence
1.4
1.2
1
0.8
0.6
0.4
0.2
0
HeLa
KO8
H
HeLa Control
HeLa KO8
1 2 3 1 2 3
kDa
100
50
25
p97
proCatD
matCatD
I
Mature/Pro CatD
Fold change
2
1.5
1
0.5
0
HeLa
KO8

Fig S12

A

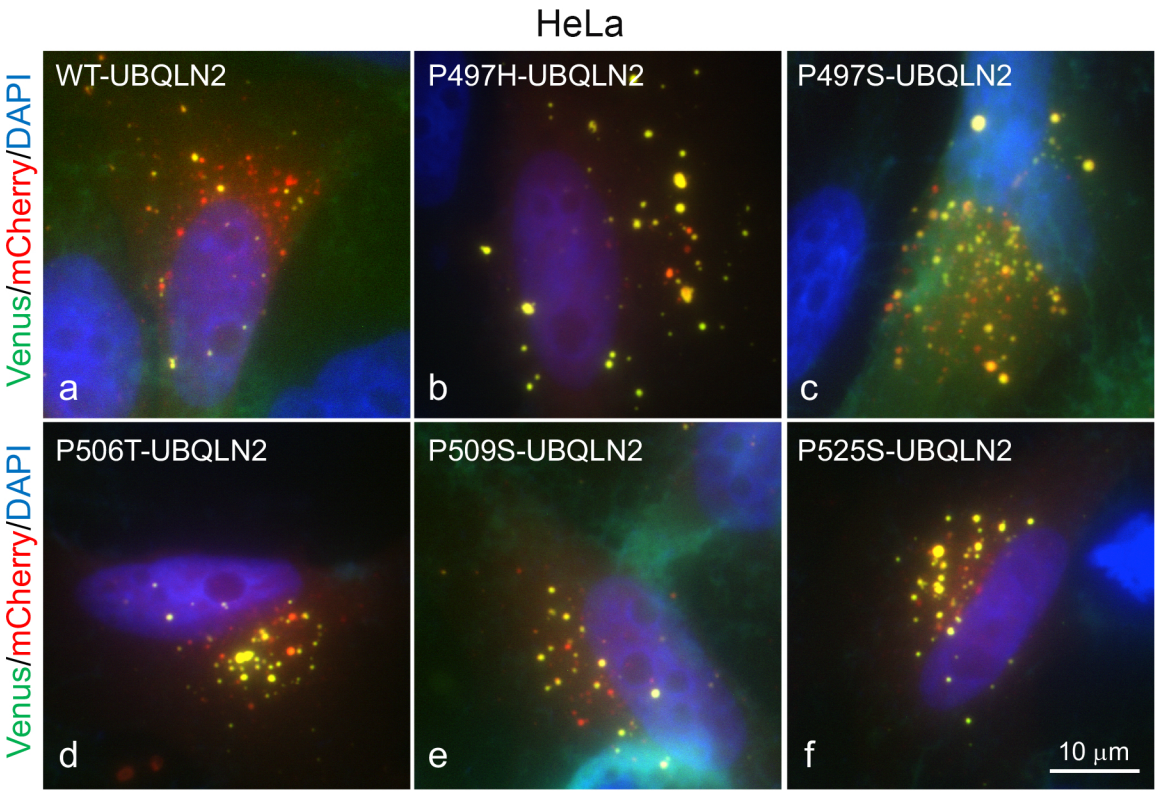
HeLa
WT-UBQLN2
P497H-UBQLN2
P497S-UBQLN2
P506T-UBQLN2
P509S-UBQLN2
P525S-UBQLN2
Venus/mCherry/DAPI
Venus/mCherry/DAPI
a
b
c
d
e
f
10 μm

B

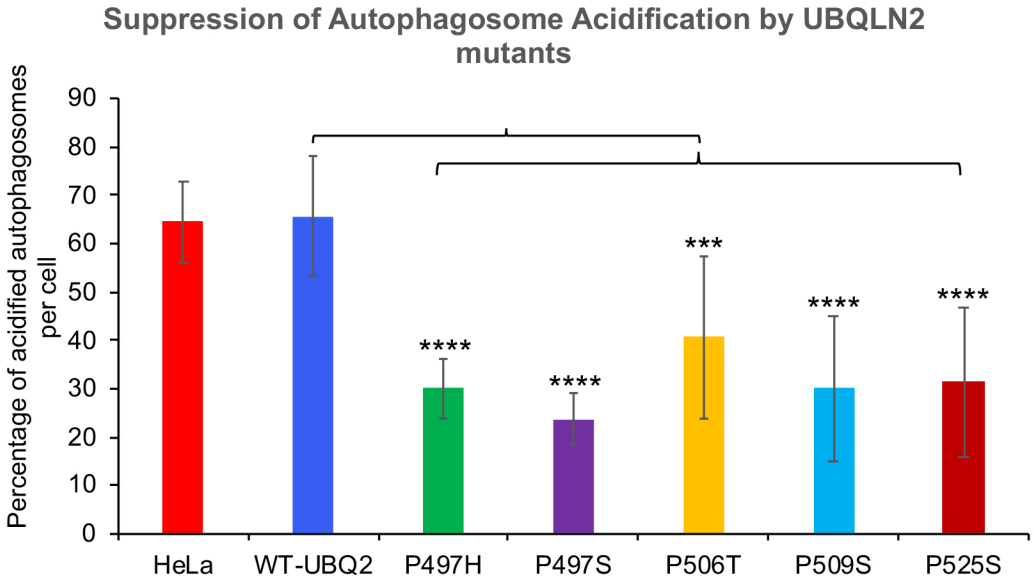
Suppression of Autophagosome Acidification by UBQLN2 mutants
Percentage of acidified autophagosomes per cell
0
10
20
30
40
50
60
70
80
90
****
****
***
****
****
HeLa
WT-UBQ2
P497H
P497S
P506T
P509S
P525S

Fig S13

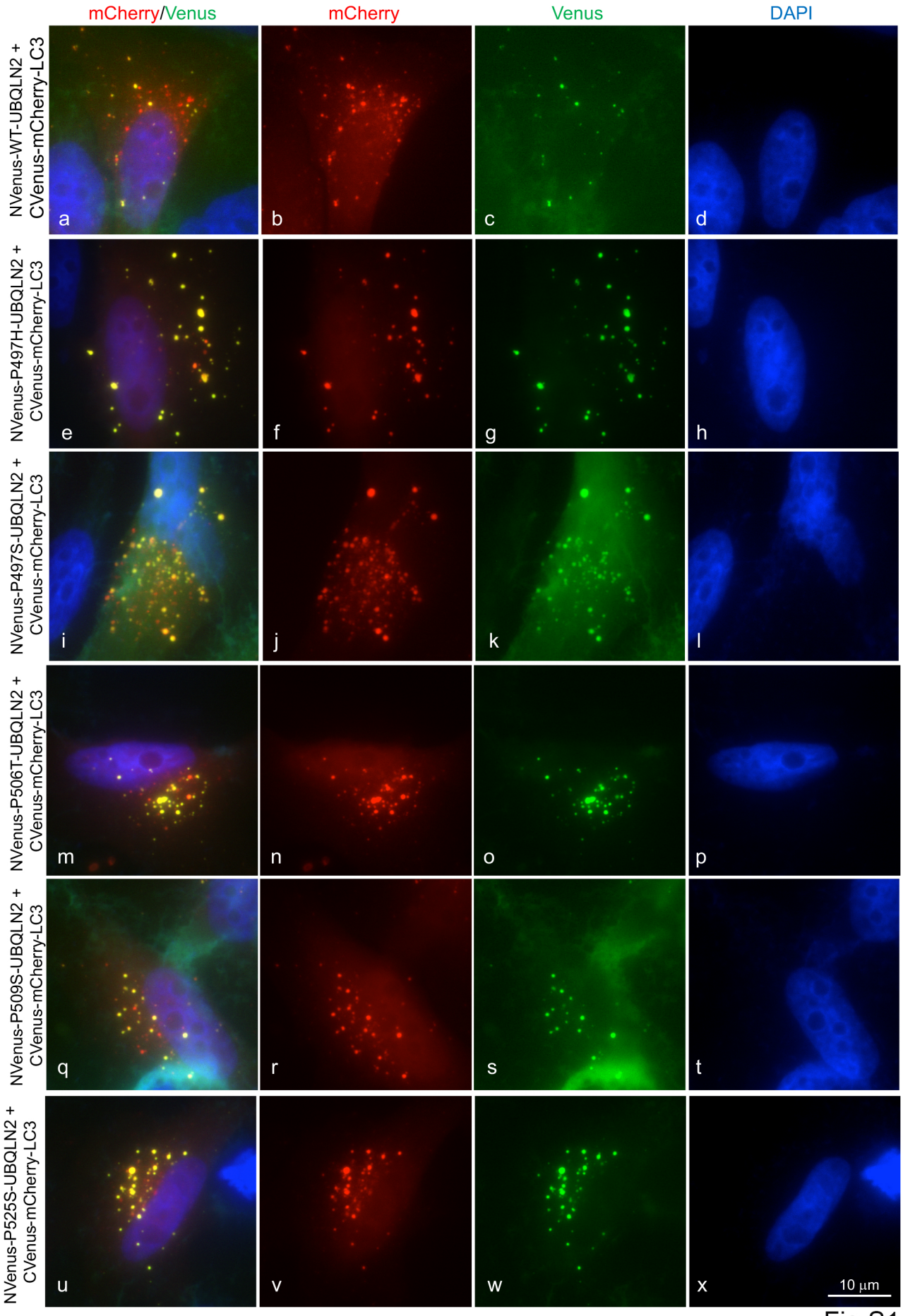
mCherry/Venus
mCherry
Venus
DAPI
NVenus-WT-UBQLN2 + CVenus-mCherry-LC3
NVenus-P497H-UBQLN2 + CVenus-mCherry-LC3
NVenus-P497S-UBQLN2 + CVenus-mCherry-LC3
NVenus-P506T-UBQLN2 + CVenus-mCherry-LC3
NVenus-P509S-UBQLN2 + CVenus-mCherry-LC3
NVenus-P525S-UBQLN2 + CVenus-mCherry-LC3
a
b
c
d
e
f
g
h
i
j
k
l
m
n
o
p
q
r
s
t
u
v
w
x
10 μm

Fig S14

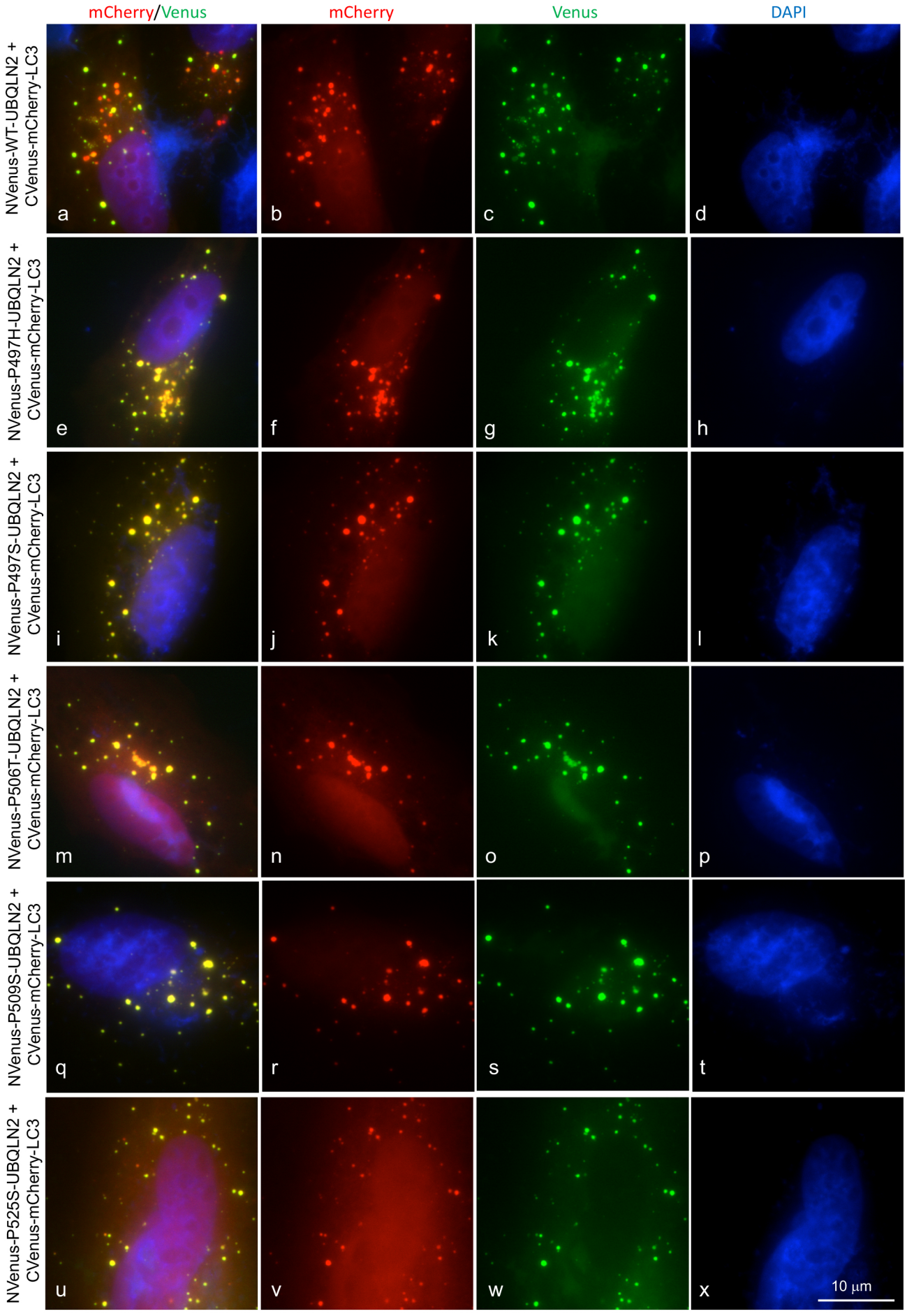
mCherry/Venus
mCherry
Venus
DAPI
NVenus-WT-UBQLN2 + CVenus-mCherry-LC3
NVenus-P497H-UBQLN2 + CVenus-mCherry-LC3
NVenus-P497S-UBQLN2 + CVenus-mCherry-LC3
NVenus-P506T-UBQLN2 + CVenus-mCherry-LC3
NVenus-P509S-UBQLN2 + CVenus-mCherry-LC3
NVenus-P525S-UBQLN2 + CVenus-mCherry-LC3
a
b
c
d
e
f
g
h
i
j
k
l
m
n
o
p
q
r
s
t
u
v
w
x
10 μm

Fig S15

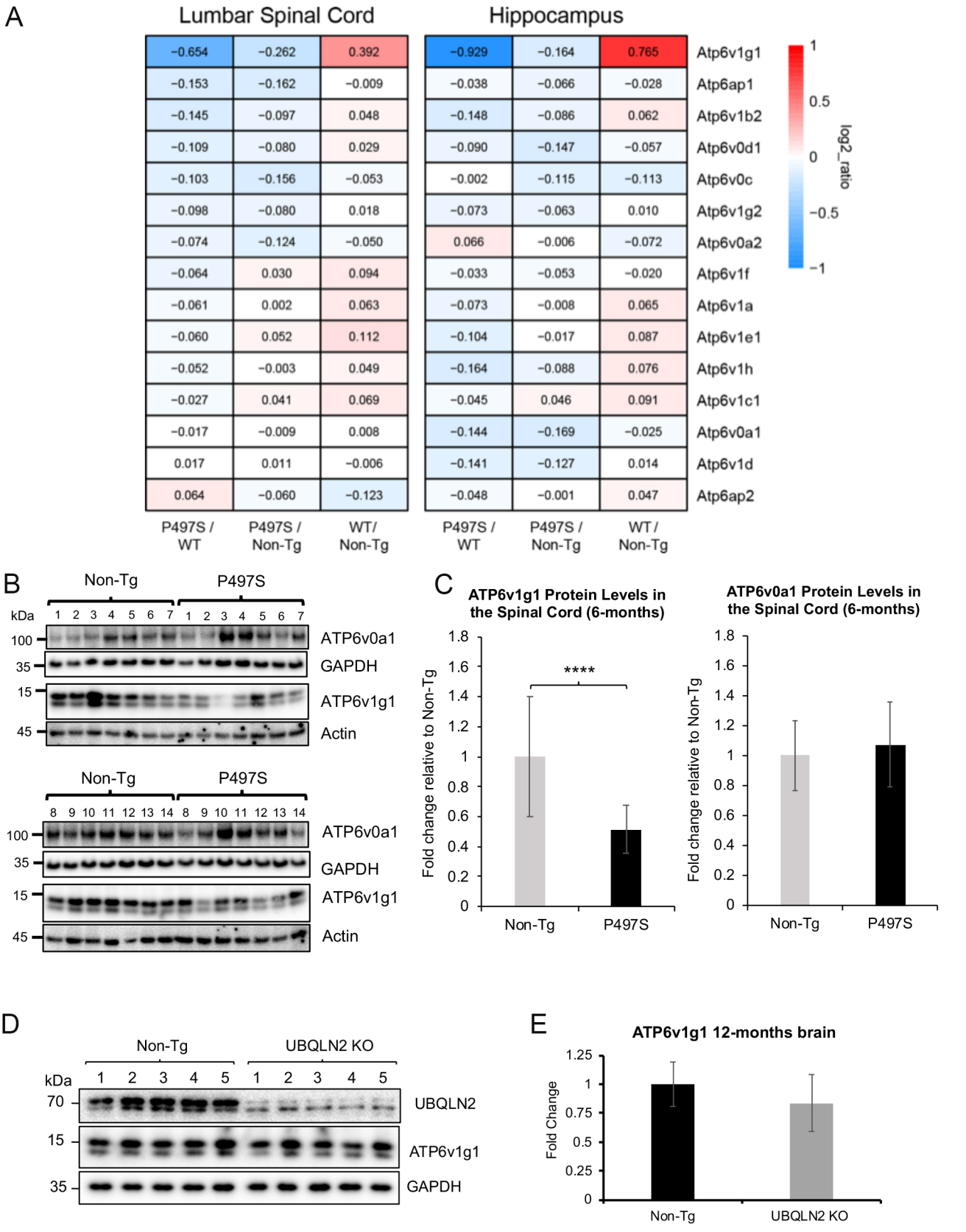
A
Lumbar Spinal Cord
Hippocampus
−0.654 −0.262 0.392 −0.929 −0.164 0.765 Atp6v1g1
−0.153 −0.162 −0.009 −0.038 −0.066 −0.028 Atp6ap1
−0.145 −0.097 0.048 −0.148 −0.086 0.062 Atp6v1b2
−0.109 −0.080 0.029 −0.090 −0.147 −0.057 Atp6v0d1
−0.103 −0.156 −0.053 −0.002 −0.115 −0.113 Atp6v0c
−0.098 −0.080 0.018 −0.073 −0.063 0.010 Atp6v1g2
−0.074 −0.124 −0.050 0.066 −0.006 −0.072 Atp6v0a2
−0.064 0.030 0.094 −0.033 −0.053 −0.020 Atp6v1f
−0.061 0.002 0.063 −0.073 −0.008 0.065 Atp6v1a
−0.060 0.052 0.112 −0.104 −0.017 0.087 Atp6v1e1
−0.052 −0.003 0.049 −0.164 −0.088 0.076 Atp6v1h
−0.027 0.041 0.069 −0.045 0.046 0.091 Atp6v1c1
−0.017 −0.009 0.008 −0.144 −0.169 −0.025 Atp6v0a1
0.017 0.011 −0.006 −0.141 −0.127 0.014 Atp6v1d
0.064 −0.060 −0.123 −0.048 −0.001 0.047 Atp6ap2
P497S / WT
P497S / Non-Tg
WT / Non-Tg
P497S / WT
P497S / Non-Tg
WT / Non-Tg
1
0.5
0
−0.5
−1
log2_ratio
B
Non-Tg
P497S
kDa
1 2 3 4 5 6 7 1 2 3 4 5 6 7
100
35
15
45
ATP6v0a1
GAPDH
ATP6v1g1
Actin
Non-Tg
P497S
8 9 10 11 12 13 14 8 9 10 11 12 13 14
100
35
15
45
ATP6v0a1
GAPDH
ATP6v1g1
Actin
C
ATP6v1g1 Protein Levels in the Spinal Cord (6-months)
Fold change relative to Non-Tg
1.8
1.6
1.4
1.2
1
0.8
0.6
0.4
0.2
0
****
Non-Tg
P497S
ATP6v0a1 Protein Levels in the Spinal Cord (6-months)
Fold change relative to Non-Tg
1.8
1.6
1.4
1.2
1
0.8
0.6
0.4
0.2
0
Non-Tg
P497S
D
Non-Tg
UBQLN2 KO
kDa
1 2 3 4 5 1 2 3 4 5
70
15
35
UBQLN2
ATP6v1g1
GAPDH
E
ATP6v1g1 12-months brain
Fold Change
1.25
1
0.75
0.5
0.25
0
Non-Tg
UBQLN2 KO

Fig S16

A

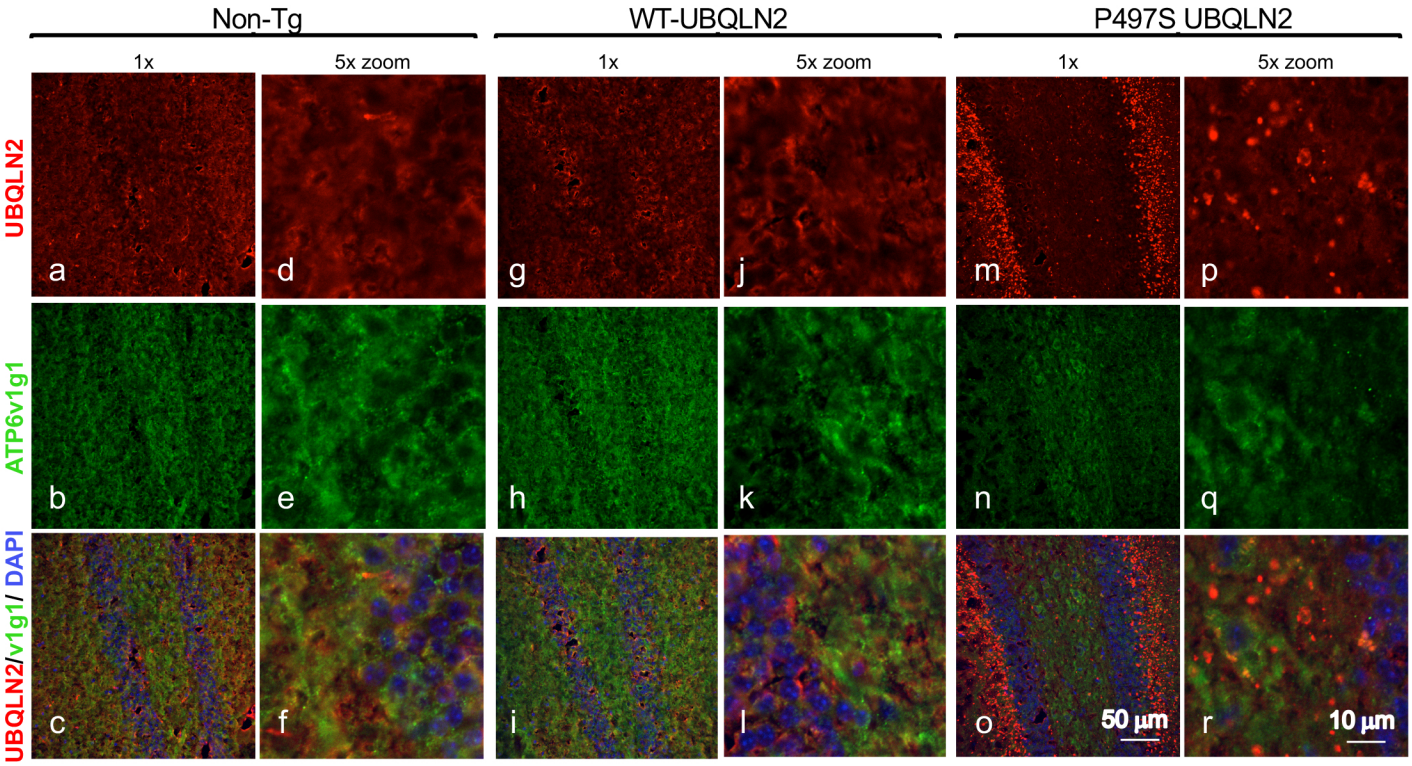
Non-Tg
WT-UBQLN2
P497S UBQLN2
1x
5x zoom
1x
5x zoom
1x
5x zoom
UBQLN2
ATP6v1g1
UBQLN2/v1g1/ DAPI
a
b
c
d
e
f
g
h
i
j
k
l
m
n
o
p
q
r
50 µm
10 µm

Fig S17

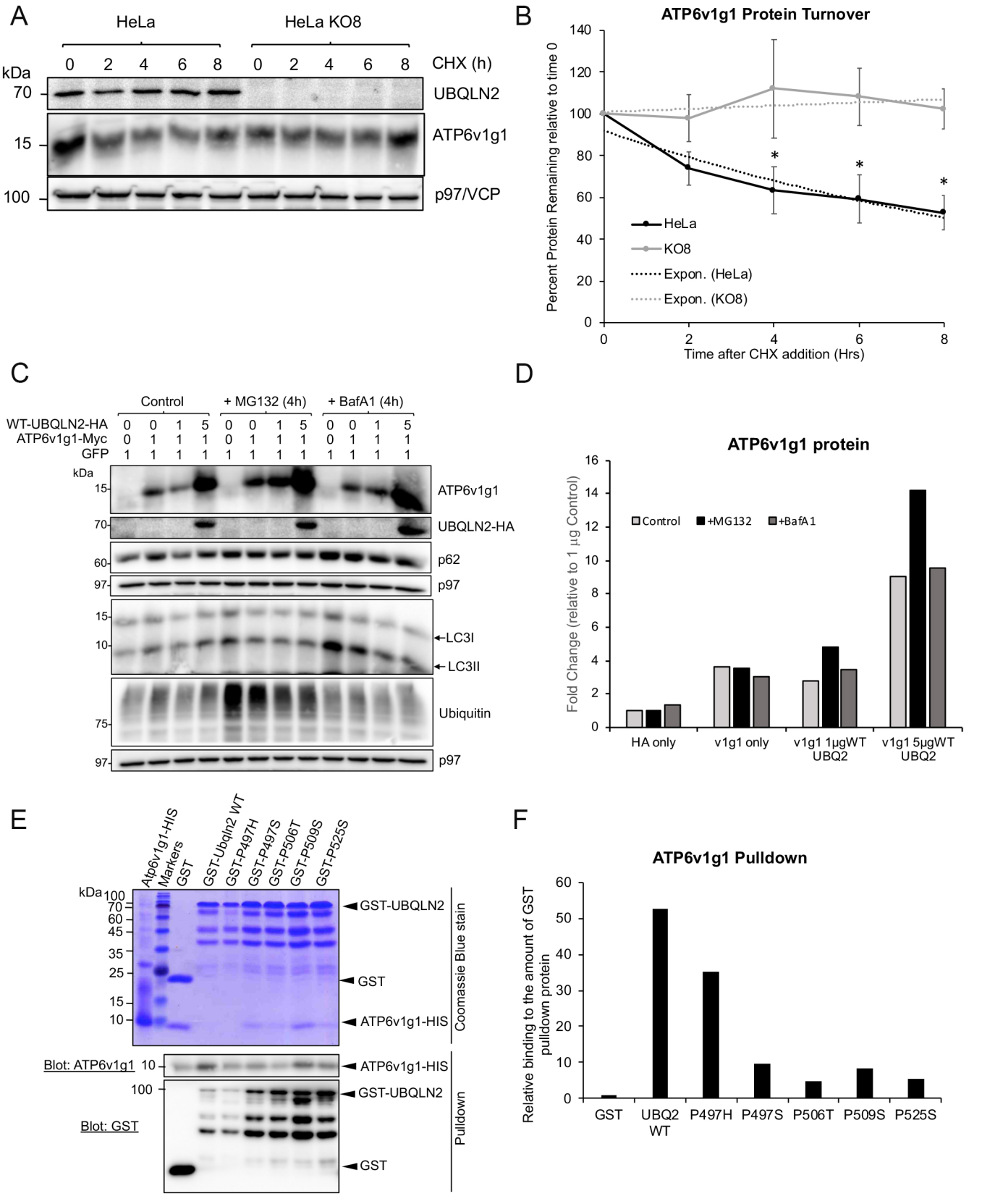
A
HeLa
HeLa KO8
0 2 4 6 8 0 2 4 6 8
CHX (h)
kDa
70
UBQLN2
15
ATP6v1g1
100
p97/VCP
B
ATP6v1g1 Protein Turnover
Percent Protein Remaining relative to time 0
Time after CHX addition (Hrs)
HeLa
KO8
Expon. (HeLa)
Expon. (KO8)
C
Control
+ MG132 (4h)
+ BafA1 (4h)
WT-UBQLN2-HA
ATP6v1g1-Myc
GFP
ATP6v1g1
UBQLN2-HA
p62
p97
LC3I
LC3II
Ubiquitin
p97
D
ATP6v1g1 protein
Fold Change (relative to 1 µg Control)
Control
+MG132
+BafA1
HA only
v1g1 only
v1g1 1µgWT UBQ2
v1g1 5µgWT UBQ2
E
Atp6v1g1-HIS
Markers
GST
GST-Ubqln2 WT
GST-P497H
GST-P497S
GST-P506T
GST-P509S
GST-P525S
kDa
GST-UBQLN2
GST
ATP6v1g1-HIS
Coomassie Blue stain
Blot: ATP6v1g1
Blot: GST
Pulldown
F
ATP6v1g1 Pulldown
Relative binding to the amount of GST pulldown protein
GST
UBQ2 WT
P497H
P497S
P506T
P509S
P525S

Fig S18

A

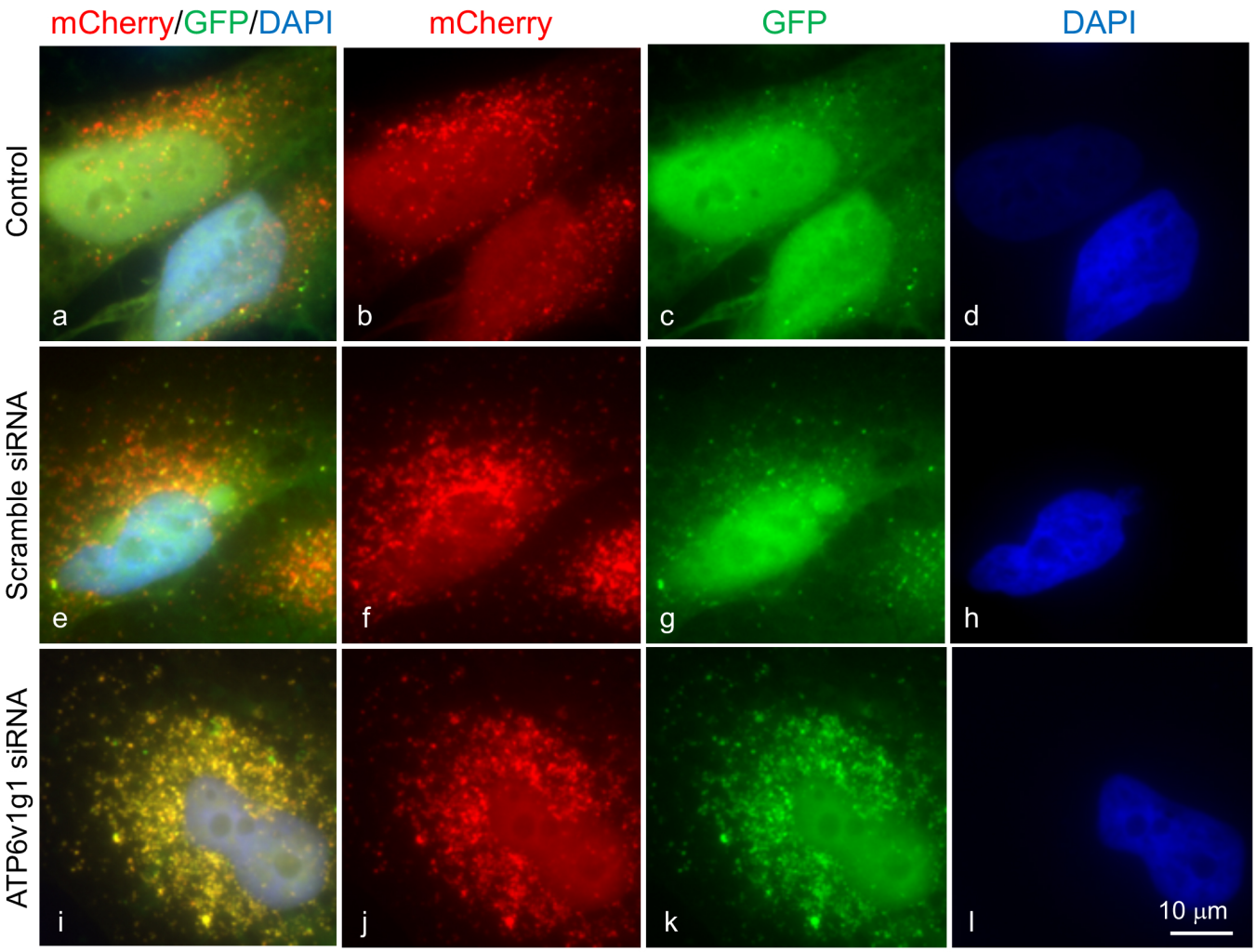
mCherry/GFP/DAPI
mCherry
GFP
DAPI
Control
Scramble siRNA
ATP6v1g1 siRNA
a
b
c
d
e
f
g
h
i
j
k
l
10 μm

Fig S19